RADIOACTIVE DECAY ENERGY DEPOSITION IN SUPERNOVAE AND THE EXPONENTIAL/QUASI-EXPONENTIAL BEHAVIOR OF LATE-TIME SUPERNOVA LIGHT CURVES

DAVID J. JEFFERY [1] [2]

Department of Physics, University of Nevada, Las Vegas

Las Vegas, Nevada 89154-4002

[1] Department of Physics, University of Nevada, Las Vegas, 4505 S. Maryland Parkway, Las Vegas, Nevada 89154-4002, email: jeffery@physics.unlv.edu

[2] Present address: Middle Tennessee State University, Department of Physics & Astronomy, Wiser-Patten Science Hall, 1301 East Main Street, Murfreesboro, Tennessee 37132

ABSTRACT

The radioactive decay energy (RDE) deposition in supernovae from the decay chain ^{56}Ni $\rightarrow ^{56}$Co $\rightarrow ^{56}$Fe usually directly powers the ultraviolet/optical/infrared (UVOIR) bolometric luminosity of supernovae in their quasi-steady state phase until very late times. The result for this phase is exponential/quasi-exponential UVOIR bolometric light curves and often exponential/quasi-exponential broad band light curves. A presentation is given of a simple, approximate, analytic treatment of RDE deposition that provides a straightforward understanding of the exponential/quasi-exponential behavior of the UVOIR bolometric luminosity and a partial understanding of the exponential/quasi-exponential behavior of the broad band light curves. The treatment reduces to using a normalized deposition function $N^*_{\rm Ni}(t)$ as an analysis tool. (The absolute deposition is determined by specifying the initial ^{56}Ni mass or fitting absolute supernova UVOIR bolometric luminosity.) The time evolution of $N^*_{\rm Ni}(t)$ is determined by three time scales: the half-lives of ^{56}Ni and ^{56}Co, and a fiducial time parameter t_0 that governs the time-varying γ-ray optical depth behavior of a supernova. The t_0 parameter can be extracted from a structural supernova model, or by fitting either the RDE deposition curve from a more detailed treatment of deposition or the observed UVOIR bolometric light curve from the quasi-steady state phase of a supernova. A t_0 parameter obtained from observations can provide a constraint on the important physical parameters of the supernova. The effective use of this constraint requires having an adequate parameterized structural supernova model.

The $N^*_{\rm Ni}(t)$ function is used to analyze the preliminary UVOIR bolometric light curve of SN Ic 1998bw (the possible cause of γ-ray burst GRB980425). The SN 1998bw fiducial time t_0 is found to be 134.42 days and a prediction is made for the evolution of the SN 1998bw RDE deposition curve and quasi-steady state UVOIR bolometric light curve out to day 1000 after the explosion. A crude estimate (perhaps a factor of a few too small) of the SN 1998bw mass obtained from a parameterized core-collapse model and $t_0 = 134.42$ days is $4.26\,M_\odot$. As further examples of the simple analytic treatment, the RDE deposition and luminosity evolution of SN Ia 1992A and SN II 1987A have also been examined.

The simple analytic treatment of RDE deposition has actually existed for 20 years at least without, apparently, being discussed at length. The main value of this paper is the explicit, detailed, general presentation of this analytic treatment.

Subject Headings: supernovae: general — supernovae: individual (SN 1992A, SN 1987A, SN 1998bw) — radiative transfer — γ-rays: theory

1. INTRODUCTION

Radioactive beta decay energy (RDE) from radioactive ^{56}Ni synthesized in the explosion and its daughter ^{56}Co is a major source of supernova luminosity. In Type Ia supernovae (SNe Ia), RDE powers the whole observable luminosity from a few days after explosion (e.g., Harkness 1991) until as far as observations extend (i.e., about 944 days after explosion for the case of SN 1992A) or so it seems (Cappellaro et al. 1997). In core-collapse supernovae (i.e., SNe II, Ib, Ic), RDE is the main source of luminosity starting from a few days to some tens of days after explosion (e.g., Woosley 1988; Young, Baron, & Branch 1995) and perhaps lasting until of order 1000 days after explosion (e.g., Suntzeff et al. 1992). Before the RDE becomes dominant, shock heat left over from the explosion is the main source. The transition time between shock heat and RDE powering depends on the parameters of the supernova, most importantly mass, kinetic energy, density profile, and composition. Circumstellar interaction and perhaps pulsar action can also supply energy to core-collapse supernovae.

In this paper we provide a simple, analytic, normalized deposition function to predict RDE deposition in supernovae as a function of time. The treatment provides a straightforward understanding of the ultraviolet/optical/infrared (UVOIR) exponential/quasi-exponential light curves and a partial understanding of the exponential/quasi-exponential broad band light curves of supernovae that occur tens to hundreds of days after explosion. The treatment is complementary to the detailed modeling of RDE deposition usually performed by Monte Carlo calculations (e.g., Höflich, Khokhlov, & Müller 1992; Swartz, Sutherland, & Harkness 1995) or, at a less detailed level, with grey (frequency-integrated) radiative transfer (by Monte Carlos or by the radiative transfer equation) (e.g., Colgate, Petschek, & Kriese 1980a, b; Swartz et al. 1995; Cappellaro et al. 1997; Jeffery 1998a, b).

The analytic treatment of RDE deposition has previously been presented by Colgate et al. (1980a, b), but only for a constant density supernova model and only briefly. We are not aware of any longer presentations. Here we present the treatment in detail and in general: i.e., we allow for any sort of homologously expanding supernova model. Special cases of supernova models are presented too.

In § 2 of this paper we briefly discuss the physics of RDE deposition and exponential/quasi-exponential light curves. Section 3 develops our RDE deposition function and parameterized structural models for SNe Ia and core-collapse supernovae. As examples of the simple analytic treatment of RDE deposition, we examine the RDE deposition and luminosity evolution of SN Ia 1992A, SN II 1987A, and SN Ic 1998bw in §§ 4, 5, and 6, respectively. Conclusions appear in § 7. Appendix A presents some useful analytic results for homologously expanding supernova models with exponential density profiles.

2. THE RDE DEPOSITION AND EXPONENTIAL/QUASI-EXPONENTIAL LIGHT CURVES

The RDE comes principally in the form of γ-rays and positrons not counting neutrinos. (Neutrinos almost entirely escape the supernova ejecta and do not contribute significantly to the RDE deposition.) The γ-ray energy that does not escape the supernova is converted to fast electron kinetic energy almost entirely by Compton scattering. The positrons lose nearly all their kinetic energy slowing down by collisions and then annihilate to form γ-rays. The lost kinetic energy and the annihilation γ-ray energy (if it does not escape) become fast electron kinetic energy also. There is also a small amount of RDE in X-rays from inner atomic orbital transitions and in the kinetic energy of ejected fast atomic electrons: both forms being a direct consequence of the nuclear decay. The X-ray energy (if it does not escape) is also converted to fast electron kinetic energy by ionizations. Although the fraction of decay energy in X-rays is very small, it is likely to become significant at very late times when Compton optical depth has become very small due to decreasing density, but X-ray optical depth is still large because of the large X-ray opacity. The ratio of the effective absorption opacities of the decay X-rays to the decay γ-rays (using 0.01 MeV as the dividing line between X-rays and γ-rays) is of order 10^3–10^4. The decay-ejected fast atomic electrons lose their kinetic

energy to other electrons, of course. In this paper we will lump the positrons and ejected atomic electrons together as positron-electron (PE) particles.

The overwhelmingly dominant decay chain for the observable epoch of most supernovae is ^{56}Ni $\rightarrow ^{56}$Co $\rightarrow ^{56}$Fe with half-lives of 6.077 ± 0.012 days and 77.27 ± 0.03 days for the first and second decays, respectively. (Half-life data in this paper is from Lawrence Berkeley National Laboratory Isotopes Project Web Data Base 1999, hereafter LBL.) The first decay releases almost all its non-neutrino energy in the form of γ-rays and the second in γ-rays and, in 19 % of the decays, in positrons (e.g., Browne & Firestone 1986; Huo 1992). The ^{56}Ni and ^{56}Co γ-ray and mean positron kinetic energy are in the range ~ 0.16–3.6 MeV (e.g., Browne & Firestone 1986; Huo 1992). The long-lived radioactive species ^{57}Co (half-life 271.79 ± 0.09 days), ^{55}Fe (half-life 2.73 ± 0.03 years), and ^{44}Ti (half-life 63 ± 3 years) are likely to become important at later times: hundreds to thousands of days after the explosion. These species (or their short-lived parents) are synthesized in comparatively small abundance in the explosion, but their long half-lives gives them importance at very late times.

The RDE converted into fast electron kinetic energy is said to be deposited. The fast electrons caused by the deposition ionize, excite, and heat the low-ionization-state supernova plasma. The deposited RDE is ultimately converted mainly into UVOIR radiation that escapes the supernova and forms the observed supernova light curves. (The complicated cascade process by which the fast electron kinetic energy gets converted into other forms of energy is discussed by, e.g., Fransson [1994, p. 688ff] and Liu & Victor [1994].) Because radioactive decay is exponential, there is a prima facie reason to expect supernova light curves to decline with time at least partially exponentially. Historically, it was the exponential (really quasi-exponential) late-time light curves of SNe Ia that first suggested radioactive sources for these supernovae (Baade et al. 1956).

Supernova light curves cannot be nearly exactly exponential in most cases for a number of reasons. For core-collapse supernovae there is the aforesaid early shock heat source, and circumstellar interaction and pulsar sources. For all supernovae, the UVOIR diffusion time scale starts out much longer than the dynamic time scale and the radioactive decay time scale. Thus, deposited RDE and shock heat energy is initially largely trapped and is released increasingly rapidly as the supernova expands and decreases in density. This early trapping rules out seeing the signature in the light curves of the ^{56}Ni decay entirely and the early signature of the ^{56}Co decay. In the case of SNe Ia, the transition to quasi-exponential light curve decline at about 60 days after explosion (or about 40 days after maximum light [i.e., B maximum]) (e.g., Leibundgut 1988; Leibundgut et al. 1991b) shows that the UVOIR trapping and the time period for processing RDE into UVOIR emission have become small. Thus a quasi-steady state has been established (or perhaps slightly later at 70 days after explosion [Pinto & Eastman 1996]) in which at any instant the entire radiative transfer of the supernova can be treated by a time-independent calculation to good accuracy. In the case of core-collapse supernovae, the transition to the quasi-steady state (exponential/quasi-exponential phase of the light curves) can occur at various times depending on the nature of progenitor, but for a massive progenitor typically at of order a hundred days after explosion as evidenced by SN 1987A (e.g., Bouchet et al. 1991; Suntzeff et al. 1991).

The late-time light curves (i.e., those from after the establishment of the quasi-steady state) are not usually truly exponential despite the effectively instantaneous conversion of RDE to UVOIR luminosity for two reasons. First, the γ-ray optical depth of the ejecta can cease to be completely trapping before or at about the same time the UVOIR optical depth becomes small. The escape of γ-rays from the ejecta adds a non-exponential factor to the RDE deposition (as we will show in §§ 3.1 and 3.2). Second, one observes light curves in particular frequency bands. Only the late-time UVOIR bolometric light curve in the case of complete γ-ray and PE particle trapping (or complete γ-ray escape and complete PE particle trapping) is guaranteed to be exponential. The individual bands receive the RDE after a more or less complicated time-dependent distribution by atomic processes.

Nevertheless, the late-time light curves of supernovae, particularly SNe Ia in the B and V bands, often appear very exponential at least in some phases when they are not in fact exponential to 1st order in those phases. We define a 1st order exponential phase to one where the logarithmic slope of a function or equivalently its instantaneous half-life (or instantaneous e-folding parameter) is constant to first order at some point in the phase. We use the expression quasi-exponential to describe phases of functions which appear very exponential without being 1st order exponential. We will adopt the convention that only light curve phases which are 1st order exponential can be considered truly exponential phases.

With older light curve data, it was often possible to fit straight lines (on semi-logarithmic plots) within the uncertainty to quasi-exponential light curves. For example, Doggett & Branch (1985) fit a straight line with a half-life of 44 days to a compilation of SN Ia blue magnitude data for days $\sim$ 120–320 after explosion: the data had a dispersion of order 1 magnitude (0.4 dex) about the line. (Here "blue" refers to a mix of bands from various older and newer magnitude systems that sample the blue side of the optical.) Barbon, Cappellaro, & Turatto (1984) found a half-life of 50 days for a line fit to another compilation of SN Ia blue magnitude data for days $\sim$ 220–420 after explosion: the magnitudes had a dispersion of order 0.5 magnitude (0.2 dex) about the line. Kirshner & Oke (1975) fit a straight line to an AB (roughly $B - 0.2$) light curve for SN Ia 1972E with a half-life of 58 days for $\sim$ 98–732 days after explosion. (We assume a rise time to maximum light of 18 days for SNe Ia: see § 4.) Older late-time blue light curve data for SNe Ia generally showed a half-life of $\sim$ 56 days (e.g., Rust, Leventhal, & McCall 1976). This order of half-life originally suggested the spontaneous fission of ^{254}Cf (half-life 60.5 ± 0.2) as a dominant energy source (Baade et al. 1956). The ^{56}Ni $\rightarrow ^{56}$Co $\rightarrow ^{56}$Fe beta decay chain for SNe Ia was put forward by Pankey (1962) and Colgate & McKee (1969). This RDE source was later accepted for core-collapse supernovae too.

Very accurate modern data shows that SNe Ia late-time light curves are not truly exponential, but have slowly decreasing logarithmic decline rates (i.e., increasing instantaneous half-lives) (e.g., Cappellaro et al. 1997). (That the older SN Ia decline half-lives cited above increase with later or longer time coverage is probably not a coincidence.) The increasing (instantaneous) half-life is easily understood qualitatively. The half-life falls below the ^{56}Co half-life because of γ-ray escape. But as the γ-ray escape increases with decreasing optical depth, the fraction of RDE deposition from the more strongly trapped PE particles increases and this eventually drives the half-life back toward the ^{56}Co half-life asymptotically. Colgate et al. (1980a, b) quantitatively demonstrated the increasing RDE deposition half-life in numerical calculations. More recently Cappellaro et al. (1997) have done the same demonstration with light curve fits to modern SN Ia data. In § 3.2, we show how both decreasing and increasing RDE deposition half-lives can arise analytically. In § 3.3, we show why the signature of increasing half-life is what one sees in the late-time light curves of SNe Ia. Both decreasing and increasing half-life phases can (but not necessarily will) have a signature in core-collapse supernova light curves (see § 3.4).

Positrons and very fast electrons can also move in supernova ejecta and can escape. They are in fact thought to be kept from traveling far by magnetic fields: possibly tangled magnetic fields. Positron transport may be an important process in supernovae and it is being actively investigated (e.g., Colgate et al. 1980a, b; Chan & Lingenfelter 1993; Cappellaro et al. 1997; Ruiz-Lapuente 1997; Milne, The, & Leising 1997; Ruiz-Lapuente & Spruit 1998). However, it is certain that positrons and fast electrons are much more strongly trapped than γ-rays. Since our interest in this paper is in studying the most basic part of RDE deposition analytically, we make the simplifying assumption that PE particle kinetic energy is deposited local to the creation of the PE particles.

At very late times, hundreds of days after explosion, the quasi-steady state is predicted to breakdown (e.g., Axelrod 1980, p. 48; Fransson & Kozma 1993; Fransson, Houck, & Kozma 1996). This is because the time scale for the fast electrons to lose energy and time scale for recombination cease to be short compared to the decay and dynamic time scales. Thus deviation from true 1st order exponential decay or quasi-steady state quasi-exponential decay in supernova light curves is to be expected for this reason if no other. There is also an observational problem at very late times. At some point an "infrared catastrophe" should occur (e.g., Axelrod 1980, p. 70; Fransson et al. 1996) in which the bulk of the emission shifts from the optical to the infrared where it is usually much less observable. Thus even if the UVOIR bolometric luminosity remains exponential/quasi-exponential, the observable light curves might show sudden, sharp declines.

3. THE RDE DEPOSITION FUNCTION

In the present case we are interested only in the global RDE deposition per unit time (i.e., the deposition function) for a supernova principally as a means for understanding supernova light curve behavior. First, we will present a fairly exact, general expression $D_{\rm g}(t)$ for deposition and show how it depends on time (§ 3.1). Then in § 3.2 we will derive $N^*_{\rm Ni}(t)$: an approximate, analytic, normalized deposition function for ^{56}Ni and its daughter ^{56}Co. It is $N^*_{\rm Ni}(t)$ and its subcomponent the absorption function $f(x)$ that are useful for analytic insight into the RDE deposition and light curve behavior. In § 3.3, we posit a parameterized

SN Ia model and in § 3.4 a parameterized core-collapse supernova model to which $N^*_{\rm Ni}(t)$ is applied.

3.1. *The Function* $D_{\rm g}(t)$

A great thing about γ-ray transfer in supernovae is that the non-scattering component of the source function (i.e., the radioactive decay source function) is independent of γ-ray transfer. This means that detailed γ-ray transfer with Compton scattering can be treated by a non-iterative Monte Carlo calculation. But a second great thing is that the actual complicated process of Compton scattering and photon degradation in energy can be approximated by a grey, pure absorption opacity treatment with an uncertainty of only a few percent at most in local and global energy absorption (Colgate et al. 1980a, b; Sutherland & Wheeler 1984; Ambwani & Sutherland 1988; Swartz et al. 1995; Jeffery 1998a, b). This means that γ-ray transfer and absorption can be reduced to simple integration and that is what we will do. We also will assume that the γ-ray transfer time can be treated as time-independent: i.e., the time scale for γ-ray transfer is much shorter than the supernova dynamical time scale and decay time scale. This assumption can begin to fail hundreds of days after explosion (e.g., Jeffery 1998b).

The radiative transfer of X-rays must be treated separately from γ-ray transfer, since X-rays face a much higher absorption opacity than γ-rays. But since the small amount of energy in X-rays is only important at very late times (hundreds of days after explosion) we will not consider them further in this section: i.e., we will not include them in the $D_{\rm g}(t)$ or $N^*_{\rm Ni}(t)$ functions.

With aforesaid simplifications an expression for $D_{\rm g}(t)$ suitable for our purposes can just be written down from simple radiative transfer:

$$D_{\rm g}(t) = \sum_i \int d^3r\, \rho(\vec{r},t)\epsilon_i \left\{ f_{\rm PE} + f_{\rm ph} \oint \frac{d\Omega}{4\pi} \left[1 - \exp\left(-\tau\right)\right] \right\}_i \ , \tag{1}$$

where the sum is over radioactive species i, the first integral is over all volume, ρ is mass density, ϵ_i is the radioactive species RDE production (not counting neutrinos which are all assumed to escape) per unit time per unit mass, $\rho\epsilon_i$ is the same except per unit volume, $f_{\rm PE}$ is the fraction of RDE (not counting neutrino energy) that goes into fast PE kinetic energy (assumed to be all locally deposited), $f_{\rm ph}$ is the fraction of RDE (counting positron annihilation energy, but not counting neutrino energy) that goes into photons, the second integral averages over all solid angle for each point $\vec{r}$, τ is the effective γ-ray absorption opacity optical depth in a given direction from $\vec{r}$ to the surface of the supernova (i.e., the optical depth of the beam path), and $(1 - e^{-\tau})$ is the absorption probability for photons that travel from $\vec{r}$ to the surface.

Supernovae after very early times are in homologous expansion where the velocities of all mass elements are constants, and the internal gas and bulk kinetic energy lost to $P\,dV$ work is negligible. (Exceptions to homologous expansion probably exist and have important consequences [e.g., Woosley 1988], but we will not consider these in this paper.) The radial position $\vec{r}$ of a mass element in homologous expansion is given by

$$\vec{r} = \vec{v}t \ , \tag{2}$$

where $\vec{v}$ is the mass element velocity and t is the time since explosion: the initial radii of the mass elements are negligible after very early times. Thus velocity can be used as a comoving coordinate. The density at any velocity decreases as t^{-3}. Therefore we can write

$$\rho(\vec{r},t) = \rho(\vec{v},t) = \rho_0(\vec{v}) \left(\frac{t_0}{t}\right)^3 \ , \tag{3}$$

where $\rho_0(\vec{v})$ is the density at $\vec{v}$ at a fiducial time t_0. Note we are not assuming spherical symmetry for the supernova.

Using the homologous condition equations (2) and (3), equation (1) can be rewritten as

$$D_{\rm g}(t) = \sum_i \int d^3v\, t_0^3 \rho_0(\vec{v})\epsilon_i \left\{ f_{\rm PE} + f_{\rm ph} \oint \frac{d\Omega}{4\pi} \left[1 - \exp\left(-\tau\right)\right] \right\}_i \ , \tag{4}$$

where the first integral is now over all velocity space volume. The deposition function now can be seen to depend on time in only two ways. First, through ϵ_i which in general is a sum of the exponential terms for radioactive species i. For beta decay from a species synthesized in the explosion

$$\epsilon_i = X_i^{\rm ini} C_i \exp\left(-t/t_{e,i}\right) \ , \tag{5}$$

where $X_i^{\rm ini}$ is initial mass fraction of species i, C_i is an energy generation rate coefficient, and $t_{e,i}$ is e-folding time (i.e., half-life divided by ln[2]). For beta decay from a species whose parent was synthesized in the explosion

$$\epsilon_i = X_{{\rm pa}(i)}^{\rm ini} B_i \left[\exp\left(-t/t_{e,i}\right) - \exp\left(-t/t_{e,{\rm pa}(i)}\right)\right] \ , \tag{6}$$

where ${\rm pa}(i)$ identifies the radioactive parent of radioactive species i, $X_{{\rm p}(i)}^{\rm ini}$ is initial mass fraction of the parent, B_i is an energy generation rate coefficient, $t_{e,i}$ is e-folding time for species i, and $t_{e,{\rm pa}(i)}$ is e-folding time for the parent. The C and B coefficients are given by

$$C_i = \frac{Q_{{\rm ph+PE},i}}{m_{\rm amu} A_i t_{e,i}} \qquad \text{and} \qquad B_i = \frac{Q_{{\rm ph+PE},i}}{m_{\rm amu} A_{{\rm pa}(i)}} \frac{1}{\left(t_{e,i} - t_{e,{\rm pa}(i)}\right)} \ , \tag{7}$$

where $Q_{{\rm ph+PE},i}$ is the mean photon plus fast PE kinetic energy per decay, A_i is atomic mass, $A_{{\rm pa}(i)}$ is the parent's atomic mass, and $m_{\rm amu}$ is the atomic mass unit (amu). For our simplified deposition treatment introduced in § 3.2, we consider only ^{56}Ni and ^{56}Co decays since these are overwhelming the most important until very late times, hundreds of days after explosion. The parameters for ^{56}Ni and ^{56}Co decays are given in Table 1.

The second time dependence of $D_{\rm g}(t)$ comes through the optical depths of the beam paths:

$$\tau = \int_{\rm em}^{\rm sur} ds\, \kappa\rho\left[\vec{v}(s), t\right] = \left(\frac{t_0}{t}\right)^2 \int_{\rm em}^{\rm sur} dv_s\, t_0 \kappa\rho_0\left[\vec{v}\,(v_s)\right] \ , \tag{8}$$

where we have used the homologous expansion condition equations (2) and (3) to get the second expression, "em" and "sur" specify the point of emission and surface, respectively, in either space or velocity, s and v_s are beam path length in physical space and velocity space, respectively, and κ is the effective absorption opacity. Note the beam path is general: i.e., not usually radial. As can be seen from equation (8), the optical depth between any two points in velocity space decreases as t^{-2}.

Swartz et al. (1995) showed for the γ-rays important in supernovae that

$$\kappa \approx \kappa_{\rm c} \mu_e^{-1} \ . \tag{9}$$

The overwhelmingly dominant γ-ray opacity in supernovae is Compton scattering (e.g., Swartz et al. 1995; Jeffery 1998b). Thus the opacity is largely determined by the number density of electrons per unit mass and this accounts for the factor of the inverse of the mean atomic mass per electron

$$\mu_e^{-1} = \sum_i \frac{X_i Z_i}{A_i} \ , \tag{10}$$

where the sum is over all elements i, X_i is mass fraction of element i, Z_i is nuclear change (since all electrons are approximately free electrons to the γ-rays important in supernovae), and A_i is again atomic mass. For ^{56}Co, the $\kappa_{\rm c}$ parameter ranges between ~ 0.05 to $0.065\,{\rm cm^2\,g^{-1}}$ and for ^{56}Ni, between ~ 0.06 to $0.1\,{\rm cm^2\,g^{-1}}$ (Swartz et al. 1995; Jeffery 1998a, b). The variation of the $\kappa_{\rm c}$ parameter depends on the global optical depth structure of the supernova: the low values are for the optically thin limit; the large values for the optically thick limit. (Note $\kappa_{\rm c}$ actually has a very weak composition dependence too that we neglect here.) We will not try to incorporate the weak, but complex, global optical depth structure dependence (and hence time dependence) of $\kappa_{\rm c}$ or variations in μ_e in our formalism directly. We will simply try to choose appropriate values of κ for the particular cases we examine and treat those values as constants for all locations and epochs.

Equation (4) would be vastly simplified if we could replace the location-, direction- and time-dependent optical depth by a mean optical depth that was only time-dependent. Given all our assumptions about γ-ray transfer, an exact mean $\bar{\tau}$ would be obtained from

$$1 - \exp\left(-\bar{\tau}\right) = \frac{\sum\limits_{i} \int d^3v\, \rho_0(\vec{v}) \epsilon_i \oint \frac{d\Omega}{4\pi} \left[1 - \exp\left(-\tau\right)\right]_i}{\sum\limits_{i} \int d^3v\, \rho_0(\vec{v}) \epsilon_i} \ . \tag{11}$$

Evaluating this exact mean $\bar{\tau}$ is, of course, tantamount to solving the exact deposition problem. We note that $\bar{\tau}$ has a complex time dependence through the ϵ_i's and the exponentials of the individual optical depths, not the simple t^{-2} time dependence of an individual optical depth given by equation (8). In the optically thin limit equation (11) reduces to

$$\bar{\tau} = \frac{\sum\limits_{i} \int d^3v\, \rho_0(\vec{v}) \epsilon_i \oint \frac{d\Omega}{4\pi} \tau_i}{\sum\limits_{i} \int d^3v\, \rho_0(\vec{v}) \epsilon_i} \ . \tag{12}$$

In this limiting case when there is a only a single radioactive species, $\bar{\tau}$ does have the simple t^{-2} time dependence since the individual τ_i's occur linearly in equation (12) and the radioactive decay time dependence cancels.

3.2. *The Function* $N^*_{\rm Ni}(t)$

So far we have developed, given the assumptions we have made, an accurate general expression for RDE deposition, $D_{\rm g}(t)$ (see § 3.1). The normalized version of $D_{\rm g}(t)$ restricted to having only ^{56}Ni at time zero is denoted $N_{\rm Ni}(t)$. We will now develop an approximate version of $N_{\rm Ni}(t)$, denoted $N^*_{\rm Ni}(t)$, by approximating some of the components of equation (4) for $D_{\rm g}(t)$ (restricted to ^{56}Ni at time zero) and normalizing. Since only a trace of ^{56}Co is produced in a supernova explosion and other radioactive species are unimportant until hundreds of days after the explosion, the assumption that there is only ^{56}Ni at time zero is excellent until very late times. The absolute deposition in a supernova model is, of course, predicted from $N^*_{\rm Ni}(t)$ or $N_{\rm Ni}(t)$ with the scale set by specifying the initial ^{56}Ni mass or by fitting the absolute UVOIR luminosity of an observed supernova.

We assume that ^{56}Ni decays to negligible abundance while the optical depth is still very large: viz., the ^{56}Ni γ-rays are completely trapped. This is a fairly good assumption for all supernovae. It begins to fail for SNe Ia which become optically thin rather quickly. But by the time the SN Ia quasi-steady state phase (which is our main interest) has begun, the ^{56}Ni is negligible. Given the complete trapping assumption for ^{56}Ni γ-rays, we replace $1 - \exp(-\tau)$ for ^{56}Ni by 1.

Note that the effective absorption opacity and thus optical depth scale for ^{56}Ni γ-rays are larger by a factor of about 1.5 in the optically thick limit than those for ^{56}Co (see § 3.1). But in qualitative discussion below, we will treat the two optical depth scales as being same.

For ^{56}Co, we approximate the time-, location-, and direction-dependent optical depth τ given by equation (8) by a location- and direction-independent characteristic optical depth

$$\tau_{\rm ch} = \tau_{\rm ch,0} \left(\frac{t_0}{t}\right)^2 = x^{-2} \ , \tag{13}$$

where $\tau_{\rm ch,0}$ is the characteristic optical depth at the fiducial time t_0 (i.e., is the fiducial [characteristic] optical depth) and

$$x = \frac{1}{\sqrt{\tau_{\rm ch,0}}} \left(\frac{t}{t_0}\right) \tag{14}$$

is a reduced time.

Since the optically thin $\bar{\tau}$ has the same time dependence as $\tau_{\rm ch}$ (assuming only ^{56}Ni at time zero), we make the optically thin $\bar{\tau}$ our choice for $\tau_{\rm ch}$ for SNe Ia and other low-mass/rapidly-expanding supernovae. These supernovae can be well observed in the γ-ray optically thin phase. If we can establish the optically thin $\bar{\tau}$ exactly, then $N^*_{\rm Ni}(t)$ will agree exactly with $N_{\rm Ni}(t)$ in the optically thin limit. For massive and/or slowly expanding core-collapse supernovae, the fully optically thin phase may be later than observations or later than the period in which the simple $N_{\rm Ni}(t)$ behavior is unperturbed by RDE deposition from sources other than ^{56}Ni and ^{56}Co. For such supernovae, $\tau_{\rm ch}$ should probably be chosen to be most characteristic of the supernova epoch one is trying to model. In order to determine the $\tau_{\rm ch}$ one needs to posit supernova models. We do this for SNe Ia and core-collapse supernovae in §§ 3.3 and 3.4, respectively.

With the aforesaid approximations and dividing through by its value at $t = 0$ (which is a maximum), equation (4) reduces to our approximate normalized deposition function

$$N^*_{\rm Ni}(t) = \exp\left(-t/t_{e,\rm Ni}\right) + G\left[\exp\left(-t/t_{e,\rm Co}\right) - \exp\left(-t/t_{e,\rm Ni}\right)\right] f[x(t)] \ , \tag{15}$$

where $G = B_{\rm Co}/C_{\rm Ni} = 0.184641$ (to more digits than significant for numerical consistency) and

$$f(x) \equiv f_{\rm PE} + f_{\rm ph}\left[1 - \exp\left(-x^{-2}\right)\right] \tag{16}$$

is what we call the absorption function (for ^{56}Co). The values of $f_{\rm PE}$ and $f_{\rm ph}$ for ^{56}Co are given in Table 1. Note that $N^*_{\rm Ni}(t)$ has only one free parameter $t_0\sqrt{\tau_{\rm ch,0}}$ which relates reduced and real time through equation (14). This parameter reduces to just t_0 because we will always set $\tau_{\rm ch,0} = 1$ since this conveniently makes t_0 roughly the time of transition between the optically thick and thin epochs.

Figure 1a shows a logarithmic plot with the deposition function $N^*_{\rm Ni}(t)$ for a range of t_0 values (with $\tau_{\rm ch,0} = 1$ of course). Figure 1b shows a logarithmic plot of the absorption function $f(x)$ and three exponential fits (which are linear on a logarithmic plot) that we discuss below.

In Figure 1a, the complete γ-ray trapping deposition curve is the curve $N^*_{\rm Ni}(t)$ approaches as $t_0 \to \infty$. After the ^{56}Ni contribution becomes negligible the complete trapping curve decays with the ^{56}Co half-life. The complete γ-ray escape deposition curve is the curve that $N^*_{\rm Ni}(t)$ approaches as $t_0 \to 0$. The complete escape curve is only a complete escape curve for ^{56}Co γ-rays: it is a complete trapping curve for ^{56}Ni γ-rays. The late-time asymptotic limit of the complete escape curve and all the curves, except for the complete trapping curve, is just $Gf_{\rm PE}\exp\left(-t/t_{e,\rm Co}\right)$ which also decays with the ^{56}Co half-life. Note that the smaller t_0, the more rapidly the ejecta becomes optically thin and faster the $N^*_{\rm Ni}(t)$ approaches the complete escape curve. We display the complete trapping and escape curves on all subsequent deposition figures for convenient reference.

The $N^*_{\rm Ni}(t)$ curves for $t_0 \lesssim t_{e,\rm Ni}$ days are not physically realistic. Supernovae with such small t_0 values (and there is no evidence that there are such supernovae) would become optically thin before the ^{56}Ni contribution had become negligible. We have assumed that ^{56}Ni becomes negligible before the complete trapping phase is over. We merely display the small t_0 cases to help demonstrate the trend with varying t_0.

An exact exponential cannot be a sum of two terms, unless they have the same e-folding parameter. Thus $N^*_{\rm Ni}(t)$ cannot be an exact exponential. However, it very closely approximates an exponential in some cases. To dispense with it at once, consider the unphysical case (given our assumptions) where $t_0 \lesssim t_{e,\rm Ni}$. In this case, the second term of equation (15) decreases quickly (after a very short growth phase from zero) and for awhile is small relative to the first term (a ^{56}Ni exponential). Thus, there will period of nearly exponential decay with almost the ^{56}Ni half-life before the ^{56}Ni exponential rather abruptly becomes negligible and $N^*_{\rm Ni}(t)$ closely approaches its late-time asymptotic limit.

The ^{56}Ni nearly-exponential phase of $N^*_{\rm Ni}(t)$ is actually not a 1st order exponential phase (see definition in § 2) although it can be very exponential for small enough t_0 as Figure 1a shows. A sum of exponentials with different e-folding parameters can only be considered a 1st order exponential if all the exponential terms, except the dominant exponential term, are exponentially small compared to the dominant term. By being exponentially small, we mean that an exponential term can be approximated by its value at infinity where it is a constant zero to all orders in a series expansion about infinity. The non-^{56}Ni exponential terms in the ^{56}Ni nearly-exponential phase are never really exponentially small compared to the ^{56}Ni exponential term even for $t_0 \to 0$. In particular, it is easy to show that the instantaneous e-folding time of the complete escape curve (the $t_0 \to 0$ case of $N^*_{\rm Ni}(t)$) is never a first order constant until the ^{56}Ni exponentials are exponentially small.

Given that ^{56}Ni is exponentially small, the sufficient condition for $N^*_{\rm Ni}(t)$ being a 1st order exponential is that $f(x)$ be either a 1st order constant or a 1st order exponential itself. The $f(x)$ function has two stationary points: a maximum of 1 at $x = 0$ and a minimum of $f_{\rm PE}$ at $x = \infty$. These give what we will call the early and late 1st order exponential phases, respectively. Both, of course, have the half-life of ^{56}Co.

In order to realize the early 1st order exponential phase the complete trapping phase for ^{56}Co γ-rays must continue after the ^{56}Ni contribution is exponentially small: i.e., $f(x)$ must not differ significantly from 1 until after the ^{56}Ni contribution is exponentially small. (Note $|\log[f(x)]| \leq 0.001$ for $x \leq 0.4$ and $f(x) > 0.99$ for $x \leq 0.46$.) In Figure 1a, only the $N^*_{\rm Ni}(t)$ deposition curve for $t_0 = 200$ days has a noticeable early 1st order exponential phase. An early 1st order exponential phase may or may not have a direct signature in light curves depending on whether or not it lasts into the quasi-steady state period.

After the ^{56}Ni contribution has become exponentially small or after the early 1st order exponential phase if it exists, $N^*_{\rm Ni}(t)$ will decline more rapidly than an exponential with ^{56}Co half-life until very late times (on the t_0 time scale) (as Fig. 1a shows) because of increasing γ-ray escape from the ejecta. But at very late times the γ-ray escape probability approaches 1 and $1 - \exp\left(-x^{-2}\right) \rightarrow x^{-2} \rightarrow 0$. Thus $f(x)$ will asymptotically approach its minimum value at infinity, $f_{\rm PE} = 0.0320$. In the asymptotic limit, deposition will be at ^{56}Co decay rate and entirely due to the decay PE particle kinetic energy which we assume to be entirely locally deposited: see § 2 for a caveat about this assumption. (Recall also that we are neglecting X-rays.) As the asymptotic limit is approached one has a late 1st order exponential phase as the curves with smaller t_0 values in Figure 1a suggest. The approach to the late 1st order exponential phase is slow on the t_0 time scale because the fractional contribution of γ-rays at late times declines only as $(t_0/t)^2$. On the time scale of the ^{56}Co half-life the approach can be slow or fast, of course, as Figure 1a shows.

Although there is no sharp transition to the late 1st order exponential phase, the time when the γ-ray and PE deposition are equal can be taken as a conventional transition $x_{\rm tr}$. When the ratio of PE to γ-ray deposition is R, the reduced time (assuming the ^{56}Ni contribution to deposition is negligible) is

$$x(R) = \sqrt{\frac{-1}{\ln\left[1 - f_{\rm PE}/\left(f_{\rm ph}R\right)\right]}} \approx \sqrt{\frac{f_{\rm ph}R}{f_{\rm PE}}} \ . \tag{17}$$

For $R = 1$, we have $x_{\rm tr} \approx 5.454099$. At $x_{\rm tr}$, $f(x)$ is 0.301030 dex (or a factor of 2) above its asymptotic value and at $2x_{\rm tr}$, 0.098007 dex (or a factor of ~ 1.25).

The slow approach to the late 1st order exponential phase gives rise to a continuum of quasi-exponential phases as Figure 1a suggests. As an example (chosen for reason: see § 4), we have fitted an exponential $K_{\rm coef} \exp\left(-x/x_e\right)$ to $f(x)$ in the x-range $[2, 3]$. The fit is shown in Figure 1b and its parameters are given in Table 2. As can be seen in Figure 1b the fit closely matches $f(x)$ over the x-range $[2, 3]$: the discrepancy between the two is always less than 0.01 dex or about 2.5 % in the x-range $[2, 3]$.

Would discrepancies from exponential behavior arising from the curvature of the $\ln\left[f(x)\right]$ function be seen in late-time supernova light curves? Late-time light curve data for the various bands from before circa 1980 often had uncertainties of order 0.5 magnitudes or 0.2 dex. Clearly, discrepancies of ~ 0.01 dex or even ~ 0.1 dex between late-time light curves and exponential fits would be hard to notice or assess for significance. As one observed for longer, larger discrepancies could arise. But the later the light curve, the fainter the supernova, the more the uncertainty in the observation. Modern, accurate late-time light curves for SNe Ia do show discrepancies from exponential behavior that are a least partly due to the non-exponential nature of $f(x)$ in its slow approach to its late asymptotic limit (e.g., Cappellaro et al. 1997; see also § 4). The logarithmic decline rates of the light curves become smaller with time. It is now recognized that the behavior of late-time SN Ia light curves from say day 60 after the explosion until very late times is only quasi-exponential.

Besides the early and late 1st order exponential phases, $N^*_{\rm Ni}(t)$ predicts that there can be a third 1st order exponential phase. This is when $f(x)$ itself becomes 1st order exponential. In Figure 1b, it can be seen that $\ln[f(x)]$ has an inflection point near $x = 1$ where the logarithmic slope becomes 1st order constant and $f(x)$ becomes a 1st order exponential. Assuming the ^{56}Ni contribution has become exponentially small, then before the inflection point the RDE deposition logarithmic decline rate increases (i.e., the instantaneous half-life decreases) and after, the RDE deposition logarithmic decline rate decreases (i.e., the instantaneous half-life increases).

The inflection point $x_{\rm infl}$ can be solved for numerically from an iteration relation obtained from the second derivative of $\ln[f(x)]$:

$$x_i = \sqrt{\left(\frac{2}{3}\right)\left[1 + \frac{f_{\rm ph}\exp\left(-x_{i-1}^{-2}\right)}{f\left(x_{i-1}\right)}\right]}\ , \tag{18}$$

where i is iteration number. One obtains $x_{\rm infl} \approx 1.040765$ and $f\left(x_{\rm infl}\right) \approx 0.615465$. The parameters for an exponential fitted to $f(x)$ at the inflection point are given in Table 2. In the x-range $[0.8, 1.35]$, the maximum deviation of $f(x)$ from the inflection point fit is ~ 0.004 dex (0.01 magnitudes). In the x-range $[0.56, 1.82]$, however, the maximum deviation has grown to ~ 0.04 dex (0.1 magnitudes).

An inflection point 1st order exponential phase will be realized in RDE deposition if ^{56}Ni abundance has become exponentially small by (for the sake of definiteness) $x \approx 1.35$ (and, of course, provided that $N^*_{\rm Ni}(t)$ adequately describes deposition). In Figure 1a, the $N^*_{\rm Ni}(t)$ deposition curves for t_0 values 200, 100, and 60 days all show inflection point 1st order exponential phases. The $t_0 = 30$ day curve does not obviously show one. The ^{56}Ni fraction of RDE production (not deposition) falls below 50 % by day 18, 20 % by day 30, 7.6 % by day 40 ($x = 4/3$ for $t_0 = 30$ day), and 1 % of the RDE at day 60. From these numbers, it is clear we would not expect much of an inflection point 1st order exponential phase for $t_0 \lesssim 30$ days.

A direct signature of a 1st order exponential RDE deposition in the light curves appears only if the supernova is in quasi-steady state phase. If there is an inflection point 1st order exponential phase entirely in the quasi-steady state phase, observers measuring a UVOIR bolometric light curve or a tracer of the same in a largish region about the inflection point would probably infer a slower exponential decline than that given by the exponential fit at the inflection point. This is because the finite uncertainty in their data would hide some of the logarithmic absorption function curvature. In Table 2 we give narrow (n), middling (m), and broad (b) inflection region fits to $f(x)$. The maximum discrepancy of these fits from $f(x)$ are ~ 0.014 dex (0.035 magnitudes), ~ 0.028 dex (0.07 magnitudes), and ~ 0.04 dex (0.1 magnitudes). All but the very best modern supernova photometry might be unable to show systematic deviations of 0.035 or 0.07 magnitudes from a straight fit to light curves. Thus a UVOIR bolometric light curve or tracer would probably appear very exponential for a period significantly longer than that of the true 1st order exponential behavior.

The parameters for the exponential fits to $f(x)$ that we have found of particular interest in this paper are collected in Table 2. In addition we have included in Table 2 the half-lives of RDE deposition from strictly ^{56}Co decay that result from the product of the ^{56}Co decay exponential with the $f(x)$ function exponential fits for the two fiducial supernova models we present in §§ 3.3 and 3.4. The models are needed to convert the half-life of a fitted exponential into a real time half-life $t^{\rm fit}_{1/2}$. The half-life of a model's RDE deposition, $t^{\rm mod}_{1/2}$, is then given by

$$t^{\rm mod}_{1/2} = \frac{t^{\rm fit}_{1/2} t_{1/2,{\rm Co}}}{t^{\rm fit}_{1/2} + t_{1/2,{\rm Co}}}\ , \tag{19}$$

where $t_{1/2,{\rm Co}}$ is the ^{56}Co half-life.

Finally, we should take stock of the accuracy of $N^*_{\rm Ni}(t)$ in comparison to $N_{\rm Ni}(t)$. First, we note that our characteristic optical depth with its simple time dependence cannot in general be the real mean optical of the ejecta discussed in § 3.1. Thus in general $N^*_{\rm Ni}(t)$ cannot be exactly $N_{\rm Ni}(t)$ at all times. For SNe Ia and other low-mass/rapidly-expanding supernovae, we have already chosen $\tau_{\rm ch}$ to be the optically thin $\bar{\tau}$. Insofar as the optically thin $\bar{\tau}$ can be determined exactly, $N^*_{\rm Ni}(t)$ with this choice of $\tau_{\rm ch}$ will be exact in the optically thin limit. On the other hand, in the optically thick limit at very early times, $N^*_{\rm Ni}(t)$ and $N_{\rm Ni}$ should be nearly exactly the same for any $\tau_{\rm ch}$ of order of the true mean optical depth since virtually all γ-rays are locally trapped.

One can plausibly expect that if $N^*_{\rm Ni}(t)$ is exactly correct in two opposite time limits, then it interpolates to good accuracy in the intervening transition epoch when $\tau_{\rm ch}$ is of order 1. Nevertheless, $N^*_{\rm Ni}(t)$ can be expected to be at its worst in this period. The reason is that the real individual optical depths of a supernova will probably range over values larger and smaller than 1 giving rise to complex location and direction varying γ-ray escape and trapping behavior that a simple optical depth prescription cannot easily mimic exactly. Without having the real $\bar{\tau}$ for the transition epoch (with its in general complex time dependence), deviations of $N^*_{\rm Ni}(t)$ from $N_{\rm Ni}(t)$ will occur. Of course, a 1st order exponential phase corresponding to the single inflection point one predicted by $N^*_{\rm Ni}(t)$ can still exist. If the supernova ejecta is smoothly varying in its

properties, a smooth transition in RDE deposition from early behavior to a late 1st order exponential phase (with ^{56}Co half-life of course) can yield a single inflection point 1st order exponential phase at some point provided the ^{56}Ni contribution becomes exponentially small soon enough. But if the ejecta has several high density clumps or shells, then the RDE deposition curve might show complex behavior with multiple inflection point exponential phases that occur as these clumps or shells make the transition from optically thick to thin at different times.

There is a case in which $N^*_{\rm Ni}(t)$ would always be exact if the effective γ-ray absorption opacity κ were a true constant. In the limit that the ^{56}Ni is confined to the exact center of a spherically symmetric supernova, $\bar{\tau}$ is the exactly the radial optical depth to the center at all epochs and hence $\bar{\tau}$ always has the simple t^{-2} time dependence. The choice of the radial optical depth from the center for $\tau_{\rm ch}$ would then cause $N^*_{\rm Ni}(t)$ to be exactly $N_{\rm Ni}(t)$. Core-collapse supernovae are expected to have their ^{56}Ni confined to the central region unless there is very extensive mixing. Thus, the exact case of $N^*_{\rm Ni}(t)$ could actually be approached if κ were constant. Unfortunately, dependence of κ on the optical depth structure of supernovae and hence on time, albeit weak, is not negligible.

3.3. *A Parameterized SN Ia Model*

In order to determine the optically thin $\bar{\tau}$ (our choice for $\tau_{\rm ch}$ for SNe Ia and other low-mass/rapidly-expanding supernovae) and relate real time t and reduced time x, we need a structural supernova model. In this section we will specify a simple parameterized structural model for SNe Ia.

Spherically symmetric hydrodynamic calculations of SN Ia explosions often (but not always) produce models with density profiles that are very exponential (i.e., inverse exponential) with velocity after homologous expansion has set in. For example, the well regarded Chandrasekhar mass SN Ia models W7 (Nomoto, Thielemann, & Yokoi 1984; Thielemann, Nomoto, & Yokoi 1986), DD4 (Woosley & Weaver 1994), and M36 (Höflich 1995, Fig. 10, but note that the density is mislabeled as energy deposition) are quite exponential with equivalent-exponential model e-folding velocities (see Appendix A, eq. [A10]) of about $2700\,{\rm km\,s^{-1}}$, $2750\,{\rm km\,s^{-1}}$, and $3000\,{\rm km\,s^{-1}}$, respectively. Such nearly-exponential density profile models have been quite successful in reproducing SN Ia spectra (e.g., Jeffery et al. 1992; Kirshner et al. 1993; Höflich 1995; Nugent et al. 1995). Therefore we will assume a spherically-symmetric, exponential density profile model (i.e., an exponential model for brevity) for our homologous epoch, parameterized SN Ia model. In Appendix A, we present a number of useful analytic results for exponential models and give a prescription for exactly exponential models (equivalent-exponential models) that can approximately replace nearly exponential hydrodynamic explosion models.

The density profile of an exponential model (for the homologous epoch) is given by

$$\rho(v,t) = \rho_{\rm ce,0}\left(\frac{t_0}{t}\right)^3 \exp\left(-v/v_e\right) = \rho_{\rm ce,0}\left(\frac{t_0}{t}\right)^3 \exp\left(-z\right)\ , \tag{20}$$

where $\rho_{\rm ce,0}$ is the central density at fiducial time t_0, v is the radial velocity, v_e is the e-folding velocity, and z is radial velocity or radial position in velocity space in units of v_e. Substituting for density from equation (20) into equation (8) and assuming the opacity κ is constant, we find for an exponential model that the γ-ray optical depth from an emission point z to the surface (which is at infinity) is

$$\tau = \tau_{\rm ce,0}\left(\frac{t_0}{t}\right)^2 \int_0^\infty dz_s\ \exp\left(-z'\right)\ , \tag{21}$$

where $\tau_{\rm ce,0}$ is the radial optical depth to the center at the fiducial time t_0 (see eq. [A16] in Appendix A for the expression), z_s is beam path velocity length in units of the e-folding velocity, and

$$z' = \sqrt{z^2 + z_s^2 + 2zz_s\mu}\ . \tag{22}$$

The μ is the cosine of the angle at the emission point between the outward radial direction and the beam propagation direction. For a beam in the outward radial direction, $\mu = 1$ and the optical depth expression reduces to

$$\tau_r = \tau_{\rm ce,0}\left(\frac{t_0}{t}\right)^2 \exp\left(-z\right)\ . \tag{23}$$

Given that there is only ^{56}Co (which was initially ^{56}Ni), equation (12) for the optically thin $\bar{\tau}$ changes for our exponential SN Ia model to

$$\bar{\tau} = \tau_{\rm ce,0} \left(\frac{t_0}{t} \right)^2 q \ , \tag{24}$$

where the q parameter is defined by

$$q = \frac{\displaystyle\int_0^\infty dz\, z^2 \exp\left(-z\right) X_{\rm Ni}^{\rm ini} \int_{-1}^{1} \frac{d\mu}{2} \int_0^\infty dz_s \, \exp\left(-z'\right)}{\displaystyle\int_0^\infty dz\, z^2 \exp\left(-z\right) X_{\rm Ni}^{\rm ini}} \ . \tag{25}$$

Note that the initial ^{56}Ni fraction is location-dependent although time-independent, of course.

A bit of analysis of equation (25) shows that when all ^{56}Ni is concentrated in the center, q has its maximum value of 1 and the optically thin $\bar{\tau}$, its maximum value of $\tau_{\rm ce,0} \left(t_0/t\right)^2$. The q parameter, in fact, acts as measure of ^{56}Ni concentration. The more the ^{56}Ni is spread to low optical depth regions, the more important the small optical depth contributions are in equation (25), and the smaller q becomes. We generalize the q parameter beyond the definition of equation (25) (which is specific to exponential models) and consider q as a general initial ^{56}Ni concentration parameter regardless of the exact supernova model. The general q is large for high concentration, small for low concentration.

To study the behavior of the (exponential model) q parameter consider the special case that the (initial) ^{56}Ni exists only between velocity radii a and b (in units of the e-folding velocity of course) and that it is a constant there. Then equation (25) reduces to

$$q = \frac{\displaystyle\int_a^b dz\, z^2 \exp\left(-z\right) \int_{-1}^{1} \frac{d\mu}{2} \int_0^\infty dz_s \, \exp\left(-z'\right)}{\displaystyle\int_a^b dz\, z^2 \exp\left(-z\right)} \ . \tag{26}$$

We have been unable to analytically solve the triple integral in the numerator of equation (26) or even find an accurate analytic approximation: crude approximate analytic solutions can be found for certain special cases. The integrations in the numerator can, however, be easily done numerically. The denominator can be solved analytically using equation (A1) in Appendix A.

Equation (26) is actually heuristically useful for SNe Ia since hydrodynamic models often show the ^{56}Ni is concentrated in a distinct layer where its abundance is overwhelmingly dominant. For example, model W7 has an initial ^{56}Ni mass fraction of over 0.5 in the range $\sim$ 3375–9750 km s^{-1}. In most of this range the mass fraction is $\sim$ 0.9. Outside of the range the mass fraction falls fairly quickly to very low values. Using the e-folding velocity 2700 km s^{-1} which is in round numbers the equivalent-exponential model e-folding velocity for model W7 (see Appendix A, eq. [A10]), we obtain from equation (26) by numerical integration $q = 0.3591$. The q value extracted from a full γ-ray transfer calculation for the model W7 (assuming model W7 is an exponential model with certain fiducial parameter values: see the description below) yields $q = 0.3308$. The difference is caused by the fact that model W7 is not exactly exponential in density (e.g., it has local density maxima at $\sim$ 9200 km s^{-1}, $\sim$ 13300 km s^{-1}, $\sim$ 15000 km s^{-1}, and cuts off sharply at $\sim$ 22000 km s^{-1}) and the ^{56}Ni mass fraction is not exactly constant inside of a sharply defined layer.

If we set a and b in equation (26) to, respectively, zero and infinity (i.e., an evenly-spread-^{56}Ni case), we obtain a $q = 0.33333326$ at the highest accuracy we have computed. This value is so close to 1/3 that it is likely that the actual q value for the evenly-spread-^{56}Ni case is exactly 1/3. We have not, however, been able to find an analytic proof. The fact that the q value for the evenly-spread-^{56}Ni case is not so different from the model W7 and approximated model W7 q values cited just above shows that the interior ^{56}Ni at large optical depth dominates the deposition in this case. Because the 1/3 value is a simple rational number that seems to be exactly correct for a particularly well defined system and is not so different from values likely to be obtained for more realistic SN Ia models, we adopt 1/3 below as our fiducial q value for our parameterized SN Ia model.

From equation (24) evaluated at the fiducial time t_0 with $\tau_{\rm ce,0}$ substituted for from equation (A16) in Appendix A, we obtain an expression for a fiducial time in terms of a fiducial characteristic optical depth

$\tau_{\rm ch,0}$ (chosen to be the optically thin $\bar{\tau}$ at the fiducial time):

$$t_0 = \sqrt{\frac{M}{8\pi}\frac{\kappa q}{\tau_{\rm ch,0}}}\,\frac{1}{v_e}\ . \tag{27}$$

We will now rewrite equation (27) in terms of fiducial values. At present Chandrasekhar mass C-O white dwarfs are favored SN Ia progenitors, and so the fiducial mass is chosen to be $1.38\,M_\odot$. Since we want our expression to be as exactly valid as possible in the optically thin phase, we set the fiducial κ to $0.025\,{\rm cm^2\,g^{-1}}$: a general good opacity value for all-metal ejecta ($\mu_e \approx 2$) in the optically thin limit (see § 3.1). We take $v_e = 2700\,{\rm km\,s^{-1}}$ which in round numbers is the equivalent-exponential model e-folding velocity for model W7 (see Appendix A, eq. [A10]): model W7 is representative of currently favored SN Ia models. The fiducial q is set to 1/3 for reasons given above. As explained in § 3.2, the fiducial $\tau_{\rm ch,0}$ is set to 1 so that t_0 is conveniently roughly the time of transition between the optically thick and thin epochs. With these choices the expression for fiducial time becomes

$$t_0 = 40.895902\ {\rm days} \times \sqrt{\left(\frac{M}{1.38\,M_\odot}\right)\left(\frac{\kappa}{0.025\,{\rm cm^2\,g^{-1}}}\right)\left(\frac{1}{\tau_{\rm ch,0}}\right)\left(\frac{q}{1/3}\right)} \times \left(\frac{2700\,{\rm km\,s^{-1}}}{v_e}\right)\ . \tag{28}$$

For numerical consistency here and throughout this paper we treat fiducial values and the solar mass unit $M_\odot = 1.9891 \times 10^{33}$ g (Lide & Frederikse 1994, p. 14-2) as nearly exact numbers. Our fiducial SN Ia model is the one that has the fiducial values and thus has fiducial time $t_0 = 40.895902$ days.

To test our $N^*_{\rm Ni}(t)$ expression and our parameterized SN Ia model, we have fitted $N^*_{\rm Ni}(t)$ to a normalized W7 RDE deposition curve calculated using a grey radiative transfer procedure and the actual model W7. The LS grey γ-ray transfer procedure (Jeffery 1998a, b) was used for the calculation. This is a free-parameter-free grey procedure that accounts crudely for the variation of effective absorption opacity with optical depth structure. The LS procedure has an uncertainty of order 10 % at most for total RDE deposition: the uncertainty vanishes in the optically thick and thin limits. For a fair comparison to $N^*_{\rm Ni}(t)$, we included only the ^{56}Ni and ^{56}Co radioactive sources and turned off X-rays in the LS procedure calculation. Because of these limitations on the RDE deposition, we call the curve computed by the LS procedure, the limited W7 deposition curve.

The fitting was done by choosing a t_0 value (with $\tau_{\rm ch,0} = 1$ as always) that made the $N^*_{\rm Ni}(t)$ equal the limited W7 deposition curve exactly on day 2000 after explosion. The day 2000 epoch is well into the optically thin phase, and so the fitted t_0 reproduces the time-varying optically thin $\bar{\tau}$ to within numerical accuracy. The fitted fiducial time $t_0 = 40.74$ days. This model W7 fiducial time is very close to the fiducial SN Ia model fiducial time 40.895902 days. Assuming model W7 is exactly an exponential model with the prescribed fiducial parameters, except for the t_0 and q values, we invert equation (28) using $t_0 = 40.74$ days to obtain $q = 0.3308$. This q cannot have exactly the interpretation dictated by the q equations (25) and (26) since model W7 is not exactly an exponential model. However, in the general, if vague, interpretation of q as a concentration parameter, the q from the fit has a useful meaning. Model W7 has roughly the same order of concentration of ^{56}Ni as the exact exponential models we considered above.

Figures 2a and 2b display the limited W7 deposition curve and the fitted $N^*_{\rm Ni}(t)$ curve to day 100 and day 500 after the explosion, respectively. The $N^*_{\rm Ni}(t)$ curve is in very close agreement with the limited W7 deposition curve and consequently is difficult to see on the Figure 2b scale. The agreement is closest at early and late times as expected: less than ~ 0.001 dex discrepancy before about day 10 and after about day 240. The only period when the discrepancy is $\gtrsim 0.01$ dex the day 15–73 period where the $N^*_{\rm Ni}(t)$ curve rises above limited W7 deposition curve with the maximum disrepancy being ~ 0.07 dex (about 18 %) at day 33. It was expected that the largest discrepancies would occur during the transition from the optically thin to thick epochs: i.e., during the phase centered on reduced time $x = 1$ (see § 3.2). For model W7 this is the period centered on about day 40 after the explosion. (Recall the uncertainty in the limited W7 deposition curve is also largest in transition period, but it is no more than of order 10 % percent.)

We have also plotted on Figures 2a and 2b the complete trapping and escape curves discussed in § 3.2. As in Figure 1a, the complete trapping curve shows the transition between the early phase where declining

^{56}Ni and increasing ^{56}Co provide the RDE and the later phase where decreasing ^{56}Co provides the RDE. As we discussed in § 3.2, ^{56}Ni contribution is truly exponentially small only by of order day 60 which is $\sim 1.5t_0$ for both the fiducial SN Ia model and model W7. Thus, these models cannot really have either an early-time nor an inflection point 1st order exponential phase in RDE deposition. For an inflection point 1st order exponential phase, the ^{56}Ni contribution must be exponentially small by of order $\sim 1.35t_0$ at about the latest. Figure 2a, examined closely, confirms the lack of a first order exponential phase centered on about $t_0 = 40$ days in the model deposition curves. Since the fiducial SN Ia model and model W7 are reasonable models for SNe Ia, we conclude that SNe Ia are very unlikely to have either an early time or an inflection point 1st order exponential phase.

Recall that the quasi-steady state of SNe Ia does not start until about day 60 after the explosion. Thus even if the early or inflection point 1st order exponential phases in RDE deposition existed, they would not have a direct signature in the light curves. Because SNe Ia are likely already in the post-inflection point epoch when the quasi-steady state phase begins, one expects to see the instantaneous half-lives of their light curves only increase with time (i.e., the logarithmic decline rates decrease with time) in the quasi-steady state phase at least until very late times. And this is in fact what observations suggest happens (e.g., Cappellaro et al. 1997; see also § 4). Comparing the deposition curves to the complete escape curve in Figure 2b shows how gradual the approach is to late 1st order exponential phase on the time scale of observations which have very rarely gone beyond 500 days.

The real time half-lives of the exponential fits to RDE deposition that result from the product of pure ^{56}Co exponential decay and the $f(x)$ function exponential fits discussed in § 3.2 and put on the real time scale using the fiducial SN Ia model t_0 are shown in Table 2. As we have seen above, the early-time and inflection point 1st order exponential phases in RDE deposition cannot be realized for the fiducial SN Ia model nor model W7 nor in all likelihood actual SNe Ia. Thus the exponential fits that correspond to those cases and similarly the fit to the x-range $[0.23, 0.53]$ cannot be realized. The half-lives corresponding to those cases are presented pro forma only. However, the exponential fits to RDE deposition for the x-ranges $[2, 3]$ and $[4, 8]$, and for the late-time limit (i.e., to the time when $x \to \infty$) are good fits (after choosing the appropriate constant coefficient for the exponential fit) to the $N^*_{\rm Ni}(t)$ and limited W7 deposition curves since they occur after the ^{56}Ni is exponentially small. The x-range $[2, 3]$ and $[4, 8]$ fits correspond to the periods $\sim$ 80–120 and $\sim$ 160–320 days, respectively, for both the fiducial SN Ia model and model W7. But these are only exponential fits to quasi-exponential phases.

Finally, we note we just needed model W7 itself not the parameterized SN Ia model in order to determine t_0 by fitting. The parameterized model did, however, predict model W7's t_0 value fairly well from reasonably chosen fiducial values. Furthermore, the parameterized model gives insight into how the deposition is determined.

3.4. *A Parameterized Core-Collapse Supernova Model*

Most supernovae Ia are fairly homogeneous in their behavior. Core-collapse supernovae are much more heterogeneous. Thus it is possible that the parameterized exponential SN Ia model presented in § 3.3 may be fairly adequate for most or all SNe Ia. But a parameterized core-collapse supernova model is likely to apply only sometimes. Here we will develop a parameterized model based on the spherically symmetric $16.2\,M_\odot$ explosion model 10H of Woosley (1988): about $14.5\,M_\odot$ of the model are ejected and about $1.7\,M_\odot$ are left in a compact remnant, presumably a neutron star. Model 10H is able to account for many of the features of SN II 1987A.

The velocity profile of model 10H in the homologous epoch is very roughly describable as linear with respect to interior mass over most of the ejecta mass: the most linear region extends over the range $\sim 4\,M_\odot$–$\sim 15\,M_\odot$ corresponding to $\sim$ 1000–4250 km s^{-1} (Woosley 1988, Fig. 12a). The rough linear relation between velocity and mass implies that density goes roughly as the inverse square of velocity over most of the ejecta mass. In the innermost region below $\sim 3\,M_\odot$ (where most of the mass was left in the compact remnant), the model 10H ejecta density decreases inward roughly speaking (Woosley 1988, Fig. 28): there is no density singularity at the center of the ejecta.

For our parameterized model in the homologous epoch, we assume all the mass is located between velocities $v_{\rm a}$ and $v_{\rm b}$, and that density goes exactly an inverse-square of velocity in this interval. Thus total

mass is given by

$$M = 4\pi \int_{v_a}^{v_b} dv\, v^2 t^3 \rho_0 \left(\frac{t_0}{t}\right)^3 \left(\frac{v_0}{v}\right)^2 = 4\pi \rho_0 t_0^3 v_0^2 \left(v_b - v_a\right) \ , \tag{29}$$

where ρ_0 is a fiducial density at a fiducial radial velocity v_0 and fiducial time t_0. The radial γ-ray optical depth from a velocity v to the surface is given by

$$\tau(v) = \int_{v}^{v_b} dv\, t\kappa\rho_0 \left(\frac{t_0}{t}\right)^3 \left(\frac{v_0}{v}\right)^2 = t^{-2}\kappa\rho_0 t_0^3 v_0^2 \left(\frac{1}{v} - \frac{1}{v_b}\right) \ , \tag{30}$$

where we have assumed κ is a constant.

We now parameterize the characteristic optical depth of the ejecta τ_{ch} by the expression

$$\tau_{ch} = \tau\left(v_a/q\right) \ , \tag{31}$$

where q is again a concentration parameter. The larger q, the smaller v_a/q, the larger τ_{ch}, and the more concentrated the initial ^{56}Ni must be in the central region of the ejecta. The chosen parameterization of τ_{ch} is, of course, based on the idea that actual mean optical depth will depend on the overall supernova parameters in roughly the same way as a radial optical depth from some velocity to the surface.

We note that if all the initial ^{56}Ni is concentrated just at the innermost physical layer (i.e., at v_a), the mean optical depth for γ-ray deposition is larger than $\tau\left(v_a\right)$. A beam of γ-rays from a point at v_a must cross a larger optical depth than $\tau\left(v_a\right)$, except in the outward and inward radial directions. Thus q can be larger than 1. This contrasts with our parameterized SN Ia model where 1 was the maximum value of q (see § 3.3).

Taking $\tau\left(v_a/q\right)$ for τ_{ch} and using equations (29) and (30), we can now solve for the time when τ_{ch} is the characteristic optical depth:

$$t = \sqrt{\frac{M}{4\pi}\frac{\kappa}{\tau_{ch}}\frac{\left[1 - \left(v_a/v_b\right)\left(1/q\right)\right]}{\left[1 - \left(v_a/v_b\right)\right]}\frac{q}{v_a v_b}} \ . \tag{32}$$

We will rewrite equation (32) in terms of fiducial values guided mainly by model 10H and SN II 1987A. For mass we use $15\,M_\odot$ which is roughly the model 10H ejected mass. The most linear region of model 10H cited above contains most, but not almost all, the model 10H mass. Thus it is difficult to select v_a and v_b based model 10H alone without considerable arbitrariness. But to fit the quasi-steady state UVOIR bolometric light curve of SN 1987A (see § 5), we select the values $v_a = 700\,\mathrm{km\,s^{-1}}$ and $v_b = 5000\,\mathrm{km\,s^{-1}}$ which give a good fit (along with our other fiducial values) while being consistent with what one might estimate from model 10H (Woosley 1988, Fig. 12a). The fit is not uniquely good, of course. In model 10H, the ^{56}Ni is confined to the lowest ejecta velocities (Woosley 1988, Fig. 4). This suggests q to be of order 1. It is clear, however, that some ^{56}Ni was mixed outward perhaps as far as halfway or more in mass fraction through the ejecta (e.g., Nomoto et al. 1994a, p. 528ff, and references therein). This suggests a q parameter less than 1, maybe much less. But for the sake of definiteness we take the fiducial $q = 1$. We again choose $\tau_{ch,0} = 1$ so that our fiducial time t_0 is conveniently roughly the time of transition between the optically thick and thin epochs (see § 3.2).

Model 10H has of order $10\,M_\odot$ of metals and helium and of order $5\,M_\odot$ of hydrogen-rich material which is presumably solar or sub-solar in metal (Woosley 1988, Figs. 4 and 17). For a mixed composition of this matter using Table 1 of Jeffery (1998a) or Table 2 of Jeffery (1998b), we find $\kappa \approx 0.04\,\mathrm{cm^2\,g^{-1}}$ for the optically thick limit and $\kappa \approx 0.03\,\mathrm{cm^2\,g^{-1}}$ for the optically thin limit. The transition, broadly speaking, from optically thick to optically thin phase of SN 1987A spans whole of the SN 1987A quasi-steady state UVOIR bolometric light curve (see § 5). Thus we take average value of the limiting opacities $0.035\,\mathrm{cm^2\,g^{-1}}$ as our fiducial κ.

With the specified fiducial values, the expression for the fiducial time is

$$\begin{aligned} t_0 = {} & 563.969041 \text{ days} \\ & \times \sqrt{\left(\frac{M}{15\,M_\odot}\right)\left(\frac{\kappa}{0.035\,\mathrm{cm^2\,g^{-1}}}\right)\left(\frac{1}{\tau_{ch,0}}\right)\left[\frac{1 - \left(v_a/v_b\right)\left(1/q\right)}{1 - \left(v_a/v_b\right)}\right]} \\ & \times \sqrt{\left(\frac{700\,\mathrm{km\,s^{-1}}}{v_a}\right)\left(\frac{5000\,\mathrm{km\,s^{-1}}}{v_b}\right)\left(\frac{q}{1}\right)} \ . \end{aligned} \tag{33}$$

The parameterized model with all the fiducial values chosen is our fiducial core-collapse model and 563.969041 days is its fiducial time.

In Figure 3 we show the fiducial model $N^*_{\rm Ni}(t)$ deposition curve. The t_0 value evaluated for the fiducial model is so large that $N^*_{\rm Ni}(t)$ will realize all the 1st order exponential and quasi-exponential RDE deposition phases discussed in § 3.2, except, of course, for the ^{56}Ni nearly-exponential phase which requires small t_0. This is because ^{56}Ni contribution to the RDE deposition will become exponentially small by of order day 60 after explosion (as discussed in § 3.2 and as best seen in Figure 2a), and at this time the ejecta is practically speaking still in the optically thick limit. The real time half-lives of the exponential fits that result from the product of pure ^{56}Co exponential decay and the $f(x)$ function exponential fits discussed in § 3.2 and put on the real time scale with the fiducial core-collapse model t_0 are shown in Table 2. All these fits (when provided with appropriate constant coefficients) are good fits to the $N^*_{\rm Ni}(t)$ deposition curve in this case.

Actual large-mass and/or slowly-expanding core-collapse supernovae may never get much beyond the early or inflection point 1st order exponential phases of $N^*_{\rm Ni}(t)$-like RDE deposition. The reason is that these phases could be so long that long-lived radioactive species may become important or the quasi-steady state period may end before the phases end. Supernova SN 1987A, for example, which we discuss in § 5 did not get past (or much past anyway) the inflection point 1st order phase before both long-lived radioactive species and time-dependent effects in the energy processing from decay to UVOIR emission became important. On the other hand, small mass and/or quickly expanding core-collapse supernovae (probably most SNe Ib and Ic) reach lower optical depth sooner and may get well past the first two 1st order exponential phases before $N^*_{\rm Ni}(t)$-like RDE deposition ends. In § 6 we consider SN Ic 1998bw as a possible example of this case.

4. SN Ia 1992A

As an example of how far simple RDE deposition calculations can take one in understanding SN Ia light curves we present a comparison in Figures 4a (days 0—250) and 4b (days 0—1000) between two normalized RDE deposition curves calculated using the LS procedure (see § 3.3) for model W7 and the V light curve of normal SN Ia 1992A. The first of the deposition curves (solid line) is a full W7 deposition curve calculated with deposition from all the significant radioactive species in model W7 and with X-ray deposition included. In Table 3 we summarize the significant radioactive decays for model W7. The other deposition curve (dotted line) is just the limited W7 deposition curve presented in § 3.3. This curve is, for our present interest, virtually the same as the $N^*_{\rm Ni}(t)$ curve fitted to model W7 (see § 3.3). The full and limited curves are in close agreement until very late times (see Fig. 4b).

At very early times, ^{55}Co and ^{57}Ni contribute significantly to the full curve although this contribution is almost invisible on the scale of Figure 4a. (The full curve is normalized by the RDE deposition of the limited curve at time zero, and so rises above 1 until about day 1.3.) At time zero, ^{55}Co and ^{57}Ni contribute about 20 % of the deposition. Their rapid decay rate is the reason for their significant contribution despite the fact that they have only trace abundance. But, of course, their rapid decay rate causes their contribution to become negligible quickly: down to to ~ 6 % by day 3 and ~ 1 % by day 8. After the ^{55}Co and ^{57}Ni abundances have become exponentially small, ^{56}Ni and ^{56}Co, and then ^{56}Co alone overwhelmingly dominate the full curve because ^{56}Ni is produced in bulk in SNe Ia unlike the other radioactive species. In model W7 the initial ^{56}Ni abundance is $0.58\,M_\odot$ and this is a typical value calculated for SNe Ia. The long-lived radioactive species, however, become more important as time passes. By day 400 the long-lived radioactive species are contributing about 3 % and the ^{56}Co X-rays about 1 % to the full curve RDE deposition. At about day 930 after explosion the long-lived radioactive species become dominant: the ^{56}Co X-rays still supplying only about 1 % of the deposition.

At day 1000 the breakdown of the full curve's deposition is as follows. Photons contribute 29.2 % and PE particle kinetic energy 70.8 %. The X-rays contribute 25.9 % and the γ-rays only 3.3 %. The ^{56}Co, ^{57}Co, and ^{55}Fe contribute 38.9 %, 56.3 %, and 4.6 %, respectively. The ^{44}Ti and its short-lived daughter ^{44}Sc contribute only 0.16 %. Because of ^{44}Ti's long half-life, however, ^{44}Ti/^{44}Sc will dominate the RDE deposition by about day 5835.

It should be emphasized that the predictions of radioactive species abundance by model W7 are uncertain on the grounds of both nuclear reaction rates and the explosive nucleosynthesis. In the case of ^{56}Ni, the uncertainty is probably small since explosive production of order $0.6\,M_\odot$ of ^{56}Ni in normal SNe Ia is well

supported by a variety of empirical evidence. The abundances of trace radioactive species do not have nearly such strong support from observations and are much less certain.

Ideally one would like to compare the RDE deposition curves to SN Ia UVOIR bolometric light curves for the quasi-steady state phase which begins at ~ 60 days after explosion. So far, however, no adequate late-time UVOIR bolometric light curves for SNe Ia have been extracted. The V light curve, however, appears to be a reasonable ersatz. It has been suggested that the bolometric correction to the V light curve from about 100 days and up to maybe 600 days after explosion is $\lesssim 0.1$—0.2 magnitudes and is relatively constant (e.g., Cappellaro et al. 1997). Therefore, as an example, we have fit the V light curve of normal SN Ia 1992A (Cappellaro et al. 1997) to our deposition curves. The V light curve for SN 1992A is one of the best observed for SNe Ia and has the latest observation of a SN Ia ever: an HST datum from 926 days after the B maximum taken by the SINS team (e.g., Kirshner et al. 1993) and reduced by Cappellaro et al. (1997).

To fit the SN 1992A V light curve we have assumed a rise time to maximum light (taken to be the B maximum by convention) of 18 days. This rise time is suggested by observational evidence. The fairly normal SN Ia 1990N was discovered at a very early phase 17.5 ± 1 days before maximum light (Leibundgut et al. 1991a). And there is empirically estimated rise time to maximum light of 17.6 ± 0.5 days for SN 1994D (another fairly normal SN Ia) (Vacca & Leibundgut 1996). Additionally, observations of cosmologically remote SNe Ia (which are usually discovered well before maximum light) suggest a typical SN Ia rise time of $\sim$ 17–18 days (Nugent et al. 1999). Variation from 18 days by a few days are expected for some SNe Ia, but this will not much affect a fit of late-time light curves to theoretical predictions. The vertical level of the V light curve was determined by fitting the V light curve by eye to the deposition curves in the range from about day 300 to day 400.

The first thing to notice in Figures 4a and 4b is that the fit from day 51 on is rather good. (The period before about day 60 [i.e., before the quasi-steady phase] is that of significant UVOIR diffusion time, and so the V light curve in that period is not expected to trace the RDE deposition directly.) The second is, of course, the discrepancies in the post-day-51 period. The V data from the days 51—109 after the explosion are systematically too high by of order 0.1 dex. The V data from days 207—451 have a dispersion about the RDE deposition curves of order 0.05 dex. The V data point from day 944 (i.e., from 926 days after maximum light) is in a phase in which the two RDE deposition curves have diverged. With its estimated uncertainty of 0.12 dex, this point is somewhat inconsistent with both of the two deposition curves.

Reasons for the discrepancies are easily found. First, the V light curve may well not be a sufficiently adequate tracer of the UVOIR bolometric light curve. This is probably at least partially the cause of the systematic difference between the days 51—109 and days 207—451 behavior. On the other hand we can improve the overall fit by replacing model W7 with fiducial time $t_0 = 40.74$ days with a model with fiducial time $t_0 = 47$ days: the days 51–109 region is better fit; the days 207-451 region is fit only slightly worse. Perhaps, a model with a t_0 value significantly larger than the t_0 value of model W7 is needed.

The dispersion of the day 207—451 data is consistent with the probable uncertainty in these data of $\lesssim 0.1$ dex (Cappellaro et al. 1997).

That the day 944 V datum is close to the RDE deposition curves at all is remarkable. The prediction for SNe Ia is that the infrared catastrophe should set in $\sim$ 400–600 days after explosion (e.g., Axelrod 1980, p. 70, 133; Fransson et al. 1996; see also § 2). This means that a V light curve fitted to the RDE deposition curve in the early quasi-steady state phase is expected to fall well below the RDE deposition curve later on when most of the UVOIR bolometric emission shifts to the infrared. Fransson et al. (1996) suggested that perhaps clumping in the ejecta or more optical emission from recombination cascades might prevent the infrared catastrophe by keeping strong emission in the optical. In addition to the infrared catastrophe, the quasi-steady state should breakdown after about day 600 (e.g., Axelrod 1980, p. 48). A third factor is that PE particle escape could reduce the UVOIR bolometric light curve below the complete PE particle trapping prediction we have made (see § 2).

Of course, not too much weight should be placed on a single isolated V datum even if it is accurate. However, there is also one very late AB band magnitude ($AB \approx B - 0.2$) for SN Ia 1972E from day 732 (again taking the rise time to maximum as 18 days) that is consistent within uncertainty with quasi-exponential decline from the day 98–434 period (Kirshner & Oke 1975). (Note the B light curve is not considered as good a tracer of the UVOIR bolometric light curve as the V light curve, but V data beyond day 434 is not available for SN 1972E.) Somehow a combination of effects seem to keep the very late-time SN Ia light curves

(out to about day 950) quasi-exponential or nearly so with respect to early late-time behavior.

We have only considered one SN Ia here as an example. There certainly are variations between late-time V light curves from different SNe Ia (e.g., Cappellaro et al. 1997). However, there are certain average SN Ia observational results that can be compared to our RDE deposition curves. Leibundgut (1988) and Leibundgut et al. (1991b) presented template light curves for SNe Ia that extend into in the early quasi-steady state phase. The half-life of an exponential fitted to the day 80–120 period of their V template is 29.4 days. The mean SN Ia light V light curve of Doggett & Branch (1985) drawn from older data has a half-life of 52 days for the period of about 160–320 days after explosion. These half-lives are in fair agreement with the half-lives of 29.23 days and 54.95 days for exponential fits to the RDE deposition for the x-ranges $[2, 3]$ (approximately days 80–120) and $[4, 8]$ (approximately days 160–320), respectively, for our fiducial SN Ia model (see Table 2). The corresponding half-lives for model W7 $N^*_{\rm Ni}(t)$ curve (which is very close agreement with our fiducial model curve) (see § 3.3) are 29.16 days and 54.88 days, respectively. The good agreement between the mean observational half-lives and the half-lives of the exponential fits to our fiducial SN Ia model and model W7 $N^*_{\rm Ni}(t)$ RDE deposition curves and the fairly good fit of the model W7 RDE deposition curves to the SN 1992A V light curve in Figures 4a and 4b suggest that model W7 and similar models are adequate average models for SNe Ia in respect to RDE deposition.

Cappellaro et al. (1997) have done a more extensive, detailed analysis of late-time SN Ia V light curves and have included positron transport in their calculations. Probably their most notable conclusion was that even normal SNe Ia could come from a range of masses. The greater masses are needed for the slowest declining SNe Ia: i.e., those whose V light curves approach the late 1st order exponential phase most slowly. That their slowest declining SNe Ia, by one measure at least (viz., the width of nebular phase iron-peak element emission lines), seem to have the lowest central concentration of initial ^{56}Ni makes the need for mass variation seem all the stronger. Recall that lower concentration of ^{56}Ni (implying smaller q and t_0) aids γ-ray escape, and so hastens the approach to the late 1st order exponential phase (see § 3.3).

Cappellaro et al. (1997), however, did not perform a detailed NLTE treatment of the conversion of RDE into UVOIR emission. Such treatments have been done (e.g., Axelrod 1980; Ruiz-Lapuente et al. 1995; Ruiz-Lapuente 1997; Liu et al. 1997; Liu, Jeffery, & Schultz 1998), but limitations, particularly in atomic data input, have limited the conclusions. More detailed, less limited NLTE treatments and better late-time observations of SNe Ia would greatly aid in determining the SN Ia nature.

5. SN II 1987A

Many detailed studies of the late-time emission of SN II 1987A have been done and these have made considerable progress in understanding this object (e.g., Woosley 1988; Bouchet et al. 1991; Suntzeff et al. 1991, 1992; Li, McCray, & Sunyaev 1993; Fransson & Kozma 1993; Nomoto et al. 1994a; Fransson et al. 1996; Suntzeff 1998, and references therein). Here we simply wish to show that the $N^*_{\rm Ni}(t)$ RDE deposition curve for our fiducial core-collapse model (see § 3.4) with fiducial time $t_0 = 563.969041$ days adequately accounts for the early late-time (i.e., the quasi-steady state) UVOIR bolometric light curve of SN 1987A.

We plot the fiducial curve in Figures 5a and 5b along with the UVOIR bolometric light curve of SN 1987A (Bouchet et al. 1991; Suntzeff et al. 1991). We have vertically adjusted the SN 1987A curve to fit the fiducial curve in day 130–200 period. The explosion epoch of SN 1987A is, of course, solidly fixed by the SN 1987A neutrino burst (Bionta et al. 1987; Hirata et al. 1987). For the day 134–432 period we have only plotted the very high accuracy bolometric data derived from spectrophotometry (Bouchet et al. 1991).

As can be seen from Figure 5a, SN 1987A very suddenly entered the quasi-steady state phase where RDE deposition equals the UVOIR bolometric light curve. The transition of the SN 1987A curve from steep decline to slow decline took place over the day 120–128 period (Suntzeff & Bouchet 1991). The early slow decline phase of the SN 1987A curve is in fact the manifestation of the early 1st order exponential phase of RDE deposition that we discussed in § 3.2. This can be seen by noting that the deposition curve in Figure 5a only slowly diverges from the complete trapping curve and only well after the ^{56}Ni deposition phase has ended. Bouchet et al. (1991) give the SN 1987A curve half-life for the day 134–300 period to be 76.0 ± 0.2 days. For the fiducial model, the day 134–300 period corresponds in reduced time to the x-range $[0.238, 0.532]$. The half-life for an exponential fit to the fiducial curve for the x-range $[0.23, 0.53]$ is 75.91 days (see Table 2). The observed and fiducial model half-lives are in good agreement.

The fiducial curve fits the SN 1987A curve very well from the beginning of the quasi-steady state phase until about day 700. Of course, we chose the parameter values for the fiducial model in order to get this good fit (see § 3.4). In reality, however, we have only shown that the $N^*_{\rm Ni}(t)$ function with a well chosen t_0 value gives a good fit. Thus, the underlying picture of ^{56}Co RDE deposition in a medium of increasing transparency is certainly adequate. However, our parameterized core-collapse model may not itself be very adequate to account for SN 1987A. But even if it were exactly right for SN 1987A, we would still not be able to determine the right parameter values without more constraints than the SN 1987A curve. Model 10H suggests some other constraints, but this is not sufficient to find a unique fit since among other things model 10H does not exactly correspond to our parameterized core-collapse supernova model (see § 3.4).

After $\sim$ 800 days after explosion, the UVOIR bolometric light curve of SN 1987A starts declining distinctly less steeply. (This change is not obvious without showing post-day-1000 data.) The change is adequately accounted for by ^{57}Co RDE deposition becoming important (e.g., Suntzeff et al. 1992) and the ending of quasi-steady state of the ejecta by the ionization freeze-out (e.g., Fransson & Kozma 1993; Fransson et al. 1996). These effects are, of course, not included in the $N^*_{\rm Ni}(t)$ function.

6. SN Ic 1998bw

Supernova SN 1998bw is a very interesting object because it is a possible cause of the γ-ray burst GRB980425 which occurred on 1998 April 25.91 (Galama et al. 1998; Iwamoto et al. 1998). It was also remarkable just as a SN Ic in being unusually bright and having very fast outer ejecta (Iwamoto et al. 1998). And the supernova showed net intrinsic polarization (Kay et al. 1988) suggesting large asymmetry (Höflich, Wheeler, & Wang 1998). Intrinsic polarization, however, is not it seems an unusual feature of core-collapse supernovae (Wang, Wheeler, & Höflich 1998).

Yet another remarkable aspect of SN 1998bw is that its BVI light curves for $\sim$ 60–185 days after explosion (almost certainly entirely in the quasi-steady state phase) are very exponential, but do not have the ^{56}Co half-life (McKenzie & Schaefer 1999). (Here we assume that GRB980425 sets the date of explosion. From early-time light curve analysis of SN 1998bw, Iwamoto et al. [1998] find that the explosion epoch agrees with GRB980425 to within $+0.7/-2$ days.) As discussed in § 3.2, there is a continuum of quasi-exponential phases between the inflection point 1st order exponential phase and the late 1st order exponential phase as $t \rightarrow \infty$. The half-lives determined for exponential fits to the quasi-exponential phases will not be the ^{56}Co half-life. At first one might suppose that the SN 1998bw light curves for the day 60–185 period are from a quasi-exponential phase. The light curves, however, appear truly exponential, not just quasi-exponential. Over the day 60–185 period, the data with uncertainty of $\lesssim$0.1 magnitudes ($\lesssim$0.04 dex) shows perhaps only a slight trace of curvature on a semi-logarithmic plot and that trace has been deemed insignificant (McKenzie & Schaefer 1999, Fig. 1).

It may be in the SN 1998bw case that the light curves are showing the signature of the inflection point 1st order exponential phase of RDE deposition that occurs near $t = t_0$ (see § 3.2). Militating against this idea is the fact that the light curve half-lives are not all the same. The B, V, and I half-lives are 53.4 ± 0.8, 40.9 ± 0.7, and 41.6 ± 0.7 days, respectively. If V and I dominated the emission, then one could tentatively conclude that they trace a UVOIR bolometric light curve with a half-life of about 41 days. But spectra through day 136 show that the flux in the B band is comparable to that in the VI bands (Patat et al. 1999). The sum of different exponentials is not exactly exponential. Nevertheless it is difficult to believe that one can get close to exponentials in three bands, two of them with almost the same half-life, without the driving RDE deposition being nearly an exponential. We will assume that the UVOIR bolometric light curve for the day 60–185 period is nearly an exponential with the UVOIR bolometric light curve half-life 44 days estimated by McKenzie & Schaefer (1999).

Figure 6a shows a schematic SN 1998bw UVOIR bolometric light curve for the day 60–185 period with half-life 44 days, a fitted $N^*_{\rm Ni}(t)$ RDE deposition curve, and the complete trapping curve. The $N^*_{\rm Ni}(t)$ curve has been fitted to the schematic curve by the following procedure. The vertical level of the schematic SN 1998bw curve was determined by a least-squares fit to the $N^*_{\rm Ni}(t)$ curve. The $N^*_{\rm Ni}(t)$ curve was then varied by varying t_0 (which is $N^*_{\rm Ni}(t)$'s only free parameter when $\tau_{\rm ch,0}$ is set to 1 as it always is) in order to minimize the maximum deviation between the $N^*_{\rm Ni}(t)$ curve and the schematic SN 1998bw curve. The final fitted $N^*_{\rm Ni}(t)$ curve has a fiducial time $t_0 = 134.42$ days (for $\tau_{\rm ch,0} = 1$). The maximum deviation of

fit is 0.024 dex (0.06 magnitudes). McKenzie & Schaefer (1999) find no evidence for systematic deviations from exponential behavior in the broad band light curves over the day 60–185 period greater than 0.02 dex (0.05 magnitudes). If the actual UVOIR bolometric light curve of SN 1998bw has the same closeness to exact exponential behavior as the observed broad band light curves, then our fitted $N^*_{\rm Ni}(t)$ curve has about as much deviation from exponential behavior has can be tolerated. The maximum deviations of $N^*_{\rm Ni}(t)$ curves with fiducial times 90, 120, 150, and 180 days are 0.12 dex, 0.048 dex, 0.061 dex, and 0.11 dex, respectively. None of these curves could be tolerated given the supposed exponential behavior of the UVOIR bolometric light curve.

Our fitted $t_0 = 134.42$ days puts the inflection point of the RDE deposition at day 139.90 (see § 3.2). Thus, as we could have anticipated, a best fit to a highly exponential region of UVOIR bolometric light curve that does not have the ^{56}Co half-life can force the fitted region to be in the inflection point 1st order exponential region of the $N^*_{\rm Ni}(t)$ function. That the $N^*_{\rm Ni}(t)$ approximation tends to be weakest when time is of order t_0 (see § 3.2) is a weakness of our analysis. But a single inflection point 1st order exponential region is expected even in a more sophisticated treatment of RDE deposition provided the supernova ejecta is fairly smoothly varying and the ^{56}Ni contribution becomes exponentially small soon enough (see § 3.2).

In Figure 6b we predict RDE deposition curve and quasi-steady state UVOIR bolometric light curve out to day 1000 using $N^*_{\rm Ni}(t)$ with $t_0 = 134.42$ days. The schematic SN 1998bw curve is again displayed. The actual RDE deposition curve will probably differ from the prediction due to long-lived radioactive species; the UVOIR bolometric light curve due to those species and time-dependent effects (see § 2). The infrared catastrophe (see § 2) does not in itself cause deviations from $N^*_{\rm Ni}(t)$-like behavior in the UVOIR bolometric light curve, but it does make it harder to measure the UVOIR bolometric light curve. The predicted RDE deposition curve's approach to the complete escape curve is sufficiently slow that non-exponential behavior in the UVOIR bolometric light curve would be difficult to detect without high quality data out to several hundreds of days after explosion.

Taking our fitted $N^*_{\rm Ni}(t)$ curve at face value, we can make an estimate of the ejecta mass by inverting an expression for t_0 for a given parameterized model. We will assume the parameterized core-collapse model of § 3.4 and invert equation (33) for mass. Recall that this parameterized model assumes that the bulk of the ejecta has density going as the inverse square of velocity. Some support for this density profile for outer ejecta is provided by Branch (1999) who found that it worked well in a parameterized LTE analysis of the photospheric epoch spectra of SN 1998bw.

We now need to estimate the model parameters. From Iwamoto et al. (1998) it is known that SN 1998bw ejecta extend out to velocities $\gtrsim 28,000\,{\rm km\,s^{-1}}$. The analysis of Branch (1999) suggests ejecta velocities $\gtrsim 60,000\,{\rm km\,s^{-1}}$ and that the inverse-square density profile extends even that far. We will be more conservative and assume that the vast bulk of the ejecta is confined to an inner high-mass core as in model 10H upon which we based our parameterized core-collapse model. The estimated half-width of one emission line of the [O I] $\lambda\lambda 6300, 6364$ emission above the estimated pseudo-continuum of the day 136 nebular spectrum of SN 1998bw (Patat et al. 1999) corresponds to a velocity of order $20000\,{\rm km\,s^{-1}}$. We assume $20000\,{\rm km\,s^{-1}}$ is the outer velocity $v_{\rm b}$ of the high-mass core. Given that the analysis of Branch (1999) and that the pseudo-continuum is ill-defined, $20000\,{\rm km\,s^{-1}}$ could be a factor of 2 or 3 too small. For the inner velocity $v_{\rm a}$ of the high-mass core, we have no strong evidence. But if there was a large hollow at the center of the ejecta the unblended emission lines would tend to be flat-topped (e.g., Mihalas 1978, p. 477; Jeffery & Branch 1990, p. 190). The [O I] $\lambda\lambda 6300, 6364$ emission in the day 136 spectrum has a very sharp peak (which is probably mostly due to the strongest line), and we estimate that a low-mass, low-density center effectively setting $v_{\rm a} \gtrsim 2000\,{\rm km\,s^{-1}}$ is unlikely. We will just assume $v_{\rm a} = 700\,{\rm km\,s^{-1}}$ as we did for our fiducial core-collapse model. For the concentration factor q we choose 1 implying that the ^{56}Ni was concentrated in the innermost regions of the high-mass core. Note that Iwamoto et al. (1998) concluded that large-scale mixing of the ^{56}Ni was needed to fit the fast rise of the estimated pre-maximum SN 1998bw UVOIR bolometric light curve. The real q could be significantly less than 1. For κ we choose $0.028\,{\rm cm^2\,g^{-1}}$. This an appropriate value for all-metal ejecta in the transition phase between optically thick and thin limits as determined from Table 1 of Jeffery (1998a) or Table 2 of Jeffery (1998b). (SNe Ic are believed to have no significant hydrogen or helium.) In extracting our t_0 value from the fit to the schematic SN 1998bw curve we have already set $\tau_{\rm ch,0} = 1$ as we always do.

The expression for mass for our parameterized core-collapse model is

$$M = 15\,M_\odot \times \left(\frac{t_0}{563.969041\text{ days}}\right)^2 \left(\frac{0.035\,\text{cm}^2\,\text{g}^{-1}}{\kappa}\right) \times \left(\frac{\tau_{\text{ch},0}}{1}\right) \left[\frac{1-(v_\text{a}/v_\text{b})}{1-(v_\text{a}/v_\text{b})\,(1/q)}\right] \times \left(\frac{v_\text{a}}{700\,\text{km}\,\text{s}^{-1}}\right) \left(\frac{v_\text{b}}{5000\,\text{km}\,\text{s}^{-1}}\right) \left(\frac{1}{q}\right) \quad . \tag{34}$$

With the chosen parameter values, we obtain a mass of $4.26\,M_\odot$. Even given that our parameterized core-collapse model is appropriate for SN 1998bw, this value could be factor of few too small: v_b could be 2 or 3 times what we assume and q could significantly less than 1. The optimum v_a value could also be different from what we have assumed by a factor of 2 or more either up or down. But since our parameterized core-collapse model may not be appropriate, our mass estimate may be only order of magnitude in any case.

Other mass determinations or lower limits on mass for SN 1998bw have been given. For example, Iwamoto et al. (1998) find that a $13.8\,M_\odot$ carbon-oxygen star explosion model can reproduce fairly well estimated early-time SN 1998bw UVOIR bolometric light curve. And Branch (1999) from his photospheric epoch parameterized LTE analysis estimated that SN 1998bw had $\sim 6\,M_\odot$ above $7000\,\text{km}\,\text{s}^{-1}$. There is still, however, considerable debate about the SN 1998bw mass and structure. Given an adequate parameterized structural model for the supernova, the t_0 parameter obtained by fitting the UVOIR bolometric light curve from the quasi-steady state phase would help to constrain the supernova's mass and/or other parameters. Since SN 1998bw may be highly asymmetric, the determination of an adequate parameterized structural model may be difficult.

7. CONCLUSIONS

We have given a presentation of a simple, approximate, analytic treatment of RDE deposition in supernovae from the decay chain $^{56}\text{Ni} \rightarrow ^{56}\text{Co} \rightarrow ^{56}\text{Fe}$. The treatment provides a straightforward understanding of the exponential/quasi-exponential behavior of the UVOIR bolometric luminosity and a partial understanding of the exponential/quasi-exponential behavior of the broad band light curves. The treatment reduces to using the normalized $N^*_\text{Ni}(t)$ deposition function (see § 3.2) as an analysis tool. (The absolute deposition is determined by specifying the initial ^{56}Ni mass or fitting absolute UVOIR supernova luminosity.) The time evolution of $N^*_\text{Ni}(t)$ is determined by three time scales: the half-lives of ^{56}Ni and ^{56}Co, and a fiducial time parameter t_0 that governs the γ-ray optical depth behavior of a supernova. The t_0 parameter can be extracted from a structural supernova model, and we have shown examples of how this is done in §§ 3.3 and 3.4. It can also be obtained by fitting the RDE deposition curve from a more detailed treatment of deposition as we did in § 3.3 or by fitting to an observed UVOIR bolometric light curve from the quasi-steady state phase of a supernova as we did in §§ 5 and 6. A t_0 parameter extracted from observations can provide a constraint on the important physical parameters of a supernova. Effective use of this constraint, however, requires having an adequate parameterized structural supernova model.

The $N^*_\text{Ni}(t)$ function is used to analyze the preliminary UVOIR bolometric light curve of SN 1998bw (the possible cause of GRB980425) (§ 6). The SN 1998bw fiducial time t_0 is found to be 134.42 days and a prediction is made for the evolution of the SN 1998bw RDE deposition curve and quasi-steady state UVOIR bolometric light curve out to day 1000 after the explosion. A crude estimate (perhaps a factor of a few too small) of the SN 1998bw mass obtained from a parameterized core-collapse model and $t_0 = 134.42$ days is $4.26\,M_\odot$. As further examples of the simple analytic treatment, the RDE deposition and luminosity evolution of SN Ia 1992A and SN II 1987A have also been examined (see §§ 4 and 5).

The simple analytic treatment of RDE deposition has actually existed at least since Colgate et al. (1980a, b), but has not hitherto been given a detailed or general presentation as far as we know. The main value of this paper is the explicit, detailed, general presentation of this analytic treatment.

This work was supported by the Department of Physics of the University of Nevada, Las Vegas. I thank Enrico Cappellaro for providing me with the V light curve of SN 1992A and David Branch for his comments.

APPENDIX A

THE EXPONENTIAL DENSITY PROFILE MODEL FOR HOMOLOGOUSLY EXPANDING SUPERNOVAE

As discussed in § 3.3, hydrodynamic explosion models for SNe Ia often have density profiles in the homologous expansion epoch that are close to exponentials (i.e., inverse exponentials) as functions of radial velocity. In this appendix we present some useful analytic results for exponential density profile models for homologously expanding supernovae.

First, we note the following general integral solution that is useful in developing the analytic results:

$$I_n(z) = \int_z^\infty dz' \ (z')^n \exp(-z') = \exp(-z) \sum_{k=0}^{n} \frac{n!}{k!} z^k \ , \tag{A1}$$

where $n \geq 0$ is an integer.

Next recall that the radius r of a mass element in homologous expansion after the initial radii have become insignificant is given by

$$r = vt \ , \tag{A2}$$

where v is the mass element's radial velocity and t is the time since explosion. Recall also that the element's density at any velocity declines as t^{-3}. We will use radial velocity as comoving radial coordinate and define a dimensionless radial coordinate z by

$$z = v/v_e \ , \tag{A3}$$

where v_e is the e-folding velocity of an exponential model's density profile. The expression for the density profile can then be written

$$\rho(v,t) = \rho_{\rm ce,0} \left(\frac{t_0}{t}\right)^3 \exp(-z) \ , \tag{A4}$$

where $\rho_{\rm ce,0}$ is the central density at fiducial time t_0.

Using the equations (A1)–(A4), the expression for mass exterior to radius z for an exponential model is

$$M(z) = 4\pi t^3 \int_v^\infty dv \, v^2 \rho(v,t) = M \exp(-z) \left(1 + z + \frac{1}{2} z^2\right) \ , \tag{A5}$$

where $M = 8\pi\rho_{\rm ce,0} \left(v_e t_0\right)^3$ is total mass. Using the same equations, the expression for kinetic energy exterior to radius z is

$$\begin{aligned} E(z) &= 4\pi t^3 \int_v^\infty dv \, \frac{v^4}{2} \rho(v,t) \\ &= 6 M v_e^2 \exp(-z) \left(1 + z + \frac{1}{2} z^2 + \frac{1}{6} z^3 + \frac{1}{24} z^4\right) \ , \end{aligned} \tag{A6}$$

where $E = 48\pi\rho_{\rm ce,0} \left(v_e t_0\right)^3 v_e^2 = 6 M v_e^2$ is total kinetic energy.

It is often useful to have expressions for central density $\rho_{\rm ce,0}$, total kinetic energy E, and the ratio of total kinetic energy to total mass E/M in terms of fiducial parameter values. Since model W7 (Nomoto, Thielemann, & Yokoi 1984; Thielemann, Nomoto, & Yokoi 1986) is a widely-used standard SN Ia model whose density closely approximates an exponential, we will use it as a basis for the fiducial values. Model W7 is a Chandrasekhar mass model, and so has total mass $M = 1.38\, M_\odot$. The equivalent-exponential model v_e for model W7 in round numbers is $2700\,{\rm km\,s^{-1}}$. (We explain equivalent-exponential model below.) For a fiducial time t_0, we choose 1 day for convenience in simple calculations. (Note this fiducial time is not for the same purpose as the fiducial time we use in the main text for optical depth evolution.) Using $M = 1.38\, M_\odot$,

$v_e = 2700\,\mathrm{km\,s^{-1}}$, and $t_0 = 1\,\mathrm{day}$ as fiducial values, the desired expressions are

$$\begin{aligned}\rho_{\mathrm{ce},0} &= \frac{M}{8\pi\left(v_e t_0\right)^3} \\ &= 0.860327\times10^{-8}\,\mathrm{g\,cm^{-3}} \times \left(\frac{M}{1.38\,M_\odot}\right) \\ &\quad\times \left(\frac{2700\,\mathrm{km\,s^{-1}}}{v_e}\right)^3 \left(\frac{1\,\mathrm{day}}{t_0}\right)^3 ,\end{aligned} \tag{A7}$$

$$E = 6Mv_e^2 = 1.20064\,\mathrm{foe} \times \left(\frac{M}{1.38\,M_\odot}\right)\left(\frac{v_e}{2700\,\mathrm{km\,s^{-1}}}\right)^2 , \tag{A8}$$

and

$$\begin{aligned}\frac{E}{M} &= 6v_e^2 = 4.37400\times10^{17}\,\mathrm{ergs\,g^{-1}} \times \left(\frac{v_e}{2700\,\mathrm{km\,s^{-1}}}\right)^2 \\ &= 0.870032\,\mathrm{foe}\,M_\odot^{-1} \times \left(\frac{v_e}{2700\,\mathrm{km\,s^{-1}}}\right)^2 ,\end{aligned} \tag{A9}$$

where a foe (for ten to the fifty-one ergs) is a standard supernova energy unit of 10^{51} ergs. (Recall from the main text that for numerical consistency we treat fiducial values and the solar mass unit $M_\odot = 1.9891\times10^{33}\,\mathrm{g}$ [Lide & Frederikse 1994, p. 14-2] as nearly exact numbers.)

Since SN Ia hydrodynamic explosion models often have density profiles that are close to exponential, there is some interest in specifying exponential models that in some ways are equivalent to those explosion models: viz., equivalent-exponential models. Two parameters are needed to specify an equivalent-exponential model. The explosion model's central density and an e-folding velocity drawn from a fit to the explosion model's density profile may not be good choices for these parameters: the central density may not be representative of the overall explosion model and good criteria for obtaining the fitted e-folding velocity need to be specified. We will instead choose the explosion model's total mass M and total kinetic energy E as the parameters. Together these parameters should yield an equivalent-exponential model that globally is much like the original explosion model: the closer the explosion model is to an exponential model, the better the likeness, of course. The expression for the equivalent-exponential model e-folding velocity follows from equation (A8) or equation (9):

$$v_e = \sqrt{\frac{1}{6}\frac{E}{M}} = 2700\,\mathrm{km\,s^{-1}} \times \sqrt{\left(\frac{E}{1.20064\,\mathrm{foe}}\right)\left(\frac{1.38\,M_\odot}{M}\right)} . \tag{A10}$$

Given v_e, the central density of the equivalent-exponential model is obtainable from equation (A7).

We have calculated the equivalent-exponential model v_e for model W7 to be $2724\,\mathrm{km\,s^{-1}}$. Since the calculation depends a bit on how one integrates the kinetic energy over the finite number of zones that make up model W7, there is no real reason for using exactly $2724\,\mathrm{km\,s^{-1}}$ as a fiducial v_e value. Thus, above we chose the round number $2700\,\mathrm{km\,s^{-1}}$.

It is useful to specify a few other exponential model results. The central atom density n_{at} is given by

$$\begin{aligned}n_{\mathrm{at}} &= \frac{\rho_{\mathrm{ce},0}}{m_{\mathrm{amu}}\mu_{\mathrm{at}}} \\ &= 0.925179\times10^{14}\,\mathrm{cm^{-3}} \\ &\quad\times \left(\frac{56}{\mu_{\mathrm{at}}}\right)\left(\frac{M}{1.38\,M_\odot}\right)\left(\frac{2700\,\mathrm{km\,s^{-1}}}{v_e}\right)^3\left(\frac{1\,\mathrm{day}}{t_0}\right)^3 ,\end{aligned} \tag{A11}$$

where $m_{\mathrm{amu}} = 1.6605402(10)\times10^{-24}\,\mathrm{g}$ (Lide & Frederikse 1994, p. 1-1: uncertainty in the last digits is given in the brackets) is the atomic mass unit (amu) and μ_{at} is the mean atomic mass, and where the second expression is in terms of fiducial values. The mean atomic mass is defined by

$$\mu_{\mathrm{at}}^{-1} = \sum_i \frac{X_i}{A_i} , \tag{A12}$$

where the sum is over all elements i, X_i is the mass fraction of element i, and A_i is element i's atomic mass. Since the center of model W7 is dominated by stable ^{56}Fe (even at time zero) and this may be typical of SNe Ia, we chose the fiducial value of $\mu_{\rm at}$ to be 56, the whole number atomic mass of ^{56}Fe. Note that even if ^{56}Fe (or ^{56}Ni or ^{56}Co) do not dominate the center, iron peak elements (with A values fairly close to 56) almost certainly do.

The central free electron density $n_{\rm e}$ is given by

$$\begin{aligned} n_e &= \frac{\rho_{\rm ce,0}}{m_{\rm amu}\tilde{\mu}_{\rm e}} \\ &= 0.925179 \times 10^{14}\,{\rm cm}^{-3} \\ &\quad \times \left(\frac{56}{\tilde{\mu}_{\rm e}}\right)\left(\frac{M}{1.38\,M_\odot}\right)\left(\frac{2700\,{\rm km\,s^{-1}}}{v_e}\right)^3\left(\frac{1\,{\rm day}}{t_0}\right)^3 \ , \end{aligned} \tag{A13}$$

where $\tilde{\mu}_e$ is the mean atomic mass per free electron and where the second expression is again in terms of fiducial values. The mean atomic mass per free electron is defined by

$$\tilde{\mu}_e^{-1} = \sum_i \frac{\tilde{X}_i \tilde{Z}_i}{A_i} \ , \tag{A14}$$

where the sum is over all ions i, $\tilde{X}_i$ is the mass fraction of ion i, $\tilde{Z}_i$ is the charge on ion i, and A_i is ion i's atomic mass. Note that $\tilde{\mu}_e$ is not the same as μ_e, the mean atomic mass per electron defined by equation (10) in § 3.1: μ_e accounts for all electrons, not just free electrons. The ionization stage of the center of ejecta probably varies strongly as a function of time. But since the central iron-peak elements are likely to be at least singly ionized until very late times, it seems most convenient just to choose the singly ionized state of an $A = 56$ species as the fiducial ionization. Calculations suggest that the central iron will be mostly singly ionized at about day 300 after explosion (e.g., Ruiz-Lapuente et al. 1995; Liu et al. 1998).

For a constant opacity κ, the radial optical depth from radius z to infinity is

$$\begin{aligned} \tau(z) &= \kappa\rho_{\rm ce,0} v_e t \left(\frac{t_0}{t}\right)^3 \exp(-z) = \frac{\kappa M}{8\pi v_e^2 t^2}\exp(-z) \\ &= \tau_{\rm ce,0}\left(\frac{t_0}{t}\right)^2 \exp(-z) \ , \end{aligned} \tag{A15}$$

where $\tau_{\rm ce,0}$, defined by

$$\tau_{\rm ce,0} = \frac{\kappa M}{8\pi v_e^2 t_0^2} \ , \tag{A16}$$

is the radial optical depth to the center at the fiducial time t_0. The constant opacity γ-ray and free electron (i.e., Thomson) radial optical depths from the center to infinity in terms of the fiducial values are

$$\begin{aligned} \tau^\gamma_{\rm ce,0} &= 5017.42 \\ &\quad \times \left(\frac{\kappa}{0.025\,{\rm cm^2\,g^{-1}}}\right)\left(\frac{M}{1.38\,M_\odot}\right) \\ &\quad \times \left(\frac{2700\,{\rm km\,s^{-1}}}{v_e}\right)^2\left(\frac{1\,{\rm day}}{t_0}\right)^2 \end{aligned} \tag{A17}$$

and

$$\begin{aligned} \tau^e_{\rm ce,0} &= 1435.77 \times \left(\frac{56}{\tilde{\mu}_e}\right)\left(\frac{M}{1.38\,M_\odot}\right) \\ &\quad \times \left(\frac{2700\,{\rm km\,s^{-1}}}{v_e}\right)^2\left(\frac{1\,{\rm day}}{t_0}\right)^2 \ , \end{aligned} \tag{A18}$$

respectively. For the fiducial value of κ for γ-rays we chose $0.025\,{\rm cm^2\,g^{-1}}$ which is a good general value for the effective absorption opacity for ^{56}Co γ-rays for an all-metal medium in the optically thin limit (Swartz et al. 1995; Jeffery 1998a, b; see also § 3.1). The electron opacity is given by

$$\kappa_e = \frac{\sigma_e}{m_{\rm amu}\tilde{\mu}_e} = \frac{0.40062033}{\tilde{\mu}_e} \ , \tag{A19}$$

where $\sigma_e = 0.66524616(18) \times 10^{-24}\,\mathrm{cm}^2$ (Lide & Frederikse 1994, p. 1-2: uncertainty in the last digits is given in the brackets) is the Thomson cross section. For the fiducial value of $\tilde{\mu}_e$ we again chose 56 for niceness even though the ionization state and composition of ejecta vary widely with velocity location and the ionization state with time also.

REFERENCES

Ambwani, K., & Sutherland, P. G. 1988, ApJ, 325, 820

Axelrod, T. S. 1980, Ph.D. thesis, Univ. of California, Santa Cruz

Baade, W., Burbidge, G. R., Hoyle, F., Burbidge, E. M., Christy, R. F., & Fowler, W. A. 1956, PASP, 68, 296

Barbon, R., Cappellaro, E., & Turatto, M. 1984, A&A, 135, 27

Bhat, M. R. 1992, Nuclear Data Sheets, 67, 195

Bionta, R. M., et al. 1987, in Phys. Rev. Letters, 58, 1494

Bouchet, P., Phillips, M. M., Suntzeff, N. B., Gouiffes, C., Hanuschik, R. W., & Wooden, D. H. 1991, A&A, 245, 490

Branch 1999, in Supernovae and Gamma-Ray Bursts, ed. M. Livio, in press, astro-ph/9906168

Browne, E., & Firestone, R. B. 1986, Table of Radioactive Isotopes (New York: John Wiley & Sons, Inc.)

Cappellaro, E., Mazzali, P. A., Benetti, S., Danziger, I. J., Turatto, M., Della Valle, M., & Patat, F. 1997, A&A, 328, 203

Chan, K. W., & Lingenfelter, R. E. 1993, ApJ, 405, 614

Colgate, S. A., & McKee, C. 1969, ApJ, 157, 623

Colgate, S. A., Petschek, A. G., & Kriese, J. T. 1980a, in AIP Conference Proceedings, No. 63: Supernova Spectra, ed. R. Meyerott & G. H. Gillespie (New York: American Institute of Physics), 7

Colgate, S. A., Petschek, A. G., & Kriese, J. T. 1980b, ApJ, 237, L81

Doggett, J. B., & Branch, D. 1985, AJ, 90, 2303

Fransson, C. 1994, in Supernovae: Session LIV of the Les Houches École d'Été de Physique Théorique, ed. S. A. Bludman, R. Mochkovitch, & J. Zinn-Justin (Amsterdam: North-Holland), 677

Fransson, C., Houck, J., & Kozma, C. 1996, in Supernovae and Supernova Remnants, ed. McCray, R. (Cambridge: Cambridge University Press), 211

Fransson, C., & Kozma, C. 1993, ApJ, 408, L25

Galama, T. J., et al. 1998, Nature, 395, 670

Harkness, R. P. 1991, in ESO/EIPC Workshop: SN 1987A and Other Supernovae, ed. I. J. Danziger & K. Kjär (Garching: ESO), 447

Hirata, K., et al. 1987, in Phys. Rev. Letters, 58, 1490

Höflich, P. 1995, ApJ, 443, 89

Höflich, P., Khokhlov, A., & Müller, E. 1992, A&A, 259, 549

Höflich, P., Wheeler, J. C., & Wang, L. 1999, ApJ, submitted, astro-ph/9808086

Huo, J. 1992, Nuclear Data Sheets, 67, 523

Iwamoto, K., et al. 1998, Nature, 395, 672

Jeffery, D. J. 1998a, in Stellar Evolution, Stellar Explosions, and Galactic Chemical Evolution: Proc. 2nd Oak Ridge Symposium on Atomic & Nuclear Astrophysics, ed. A. Mezzacappa (Bristol: Institute of Physics Publishing), 687, astro-ph/9802229

Jeffery, D. J. 1998b, astro-ph/9811356

Jeffery, D. J., & Branch, D. 1990, in Jerusalem Winter School for Theoretical Physics, Vol. 6, Supernovae, ed. J. C. Wheeler, T. Piran, & S. Weinberg (Singapore: World Scientific), 149

Jeffery, D. J., Leibundgut, B., Kirshner, R. P., Benetti, S., Branch, D., & Sonneborn, G. 1992, ApJ, 397, 304

Kay, L. E., Halpern, J. P., Leighly, K. M., Heathcote, S., & Magalhaes, A. M. 1998, IAU Circ., No. 6969

Kirshner, R. P., et al. 1993, ApJ, 415, 589

Kirshner, R. P., & Oke, J. B. 1975, ApJ, 200, 574

Lawrence Berkeley National Laboratory Isotopes Project Web Data Base 1999, http://isotopes.lbl.gov/ (LBL)

Leibundgut, B. 1988, Ph.D. thesis, Univ. of Basel

Leibundgut, B., Kirshner, R. P., Filippenko, A. V., Shields, J. C., Foltz, C. B., Phillips, M. M., & Sonneborn, G. 1991a, ApJ, 371, L23

Leibundgut, B., Tammann, G. A., Cadonau, R., & Cerrito, D. 1991b, A&AS, 89, 537

Li, H., McCray, R., & Sunyaev, R. A. 1993, ApJ, 419, 824

Lide, D. R., & Frederikse, H. P. R. (ed.) 1994, CRC Handbook of Chemistry and Physics (Boca Raton: CRC Press)

Liu, W., Jeffery, D. J., & Schultz, D. R. 1998, ApJ, 494, 812

Liu, W., Jeffery, D. J., Schultz, D. R., Quinet, P., Shaw, J., & Pindzola, M. S. 1997, ApJ, 489, L141

Liu, W., & Victor, G. A. 1994, ApJ, 435, 909

McKenzie, E. H., & Schaefer, B. E. 1999, PASP, in press

Mihalas, D. 1978, Stellar Atmospheres (San Francisco: Freeman)

Milne, P. A., The, L.-S., Leising, M. D. 1997, in Proc. The Fourth Compton Symposium, ed. C. D. Dermer, M. S. Strickman, & J. D. Kurfess (New York: American Institute of Physics Press), 1022, astro-ph/9707111

Nomoto, K., Shigeyama, T., Kumagai, S., Yamaoka, H., & Suzuki, T. 1994a, in Supernovae: Session LIV of the Les Houches École d'Été de Physique Théorique, ed. S. A. Bludman, R. Mochkovitch, & J. Zinn-Justin (Amsterdam: North-Holland), 489

Nomoto, K., Thielemann, F.-K., & Yokoi, K. 1984, ApJ, 286, 644

Nomoto, K., Yamaoka, H., Shigeyama, T., Kumagai, S., & Tsujimoto, T. 1994b, in Supernovae: Session LIV of the Les Houches École d'Été de Physique Théorique, ed. S. A. Bludman, R. Mochkovitch, & J. Zinn-Justin (Amsterdam: North-Holland), 199

Nugent, P., Baron, E., Hauschildt, P. H., & Branch, D. 1995, ApJ, 441, L33

Nugent, P., et al. 1999, in preparation

Pankey, T., Jr. 1962, Ph.D. thesis, Howard University

Patat, F., et al. 1999, in preparation

Pinto, P. A., & Eastman, R. G. 1996, astro-ph/9611195

Ruiz-Lapuente, P. 1997, in Proc. NATO ASI on Thermonuclear Supernovae, ed. P. Ruiz-Lapuente, R. Canal, & J. Isern (Dordrecht: Kluwer), 681, astro-ph/9604094

Ruiz-Lapuente, P., Kirshner, R. P., Phillips, M. M., Challis, P. M., Schmidt, B. P., Filippenko, A. V., & Wheeler, J. C. 1995, ApJ, 439, 60

Ruiz-Lapuente, P., & Spruit, H. C. 1998, ApJ, 500, 360, astro-ph/9711248

Rust, B. W., Leventhal, M., & McCall, S. L. 1976, Nature, 262, 118

Suntzeff, N. B. 1998, in SN 1987A: Ten Years After: The Fifth CTIO/ESO/LCO Workshop, ed. M. M. Phillips & N. B. Suntzeff (Provo: Astr. Soc. of the Pacific), in press

Suntzeff, N. B., & Bouchet, P. 1991, in Supernovae: The Tenth Santa Cruz Workshop in Astronomy and Astrophysics, ed. S. E. Woosley (New York: Springer-Verlag), 3.

Suntzeff, N. B., Phillips, M. M., Depoy, D. L., Elias, J. H., & Walker, A. R. 1991, AJ, 102, 1118

Suntzeff, N. B., Phillips, M. M., Elias, J. H., Depoy, D. L., & Walker, A. R. 1992, ApJ, 384, L33

Sutherland, P. G., & Wheeler, J. C. 1984, ApJ, 280, 282

Swartz, D. A., Sutherland, P. G., & Harkness, R. P. 1995, ApJ, 446, 766

Thielemann, F.-K., Nomoto, K., & Yokoi, K. 1986, A&A, 158, 17

Vacca, W. D., & Leibundgut, B. 1996, ApJ, 471, L37

Wang, L., Wheeler, J. C., & Höflich, P. 1998, in SN 1987A: Ten Years After: The Fifth CTIO/ESO/LCO Workshop, ed. M. M. Phillips & N. B. Suntzeff (Provo: Astr. Soc. of the Pacific), in press

Woosley, S. E. 1988, ApJ, 330, 218

Woosley, S. E., & Weaver, T. A. 1994, in Supernovae: Session LIV of the Les Houches École d'Été de Physique Théorique, ed. S. A. Bludman, R. Mochkovitch, & J. Zinn-Justin (Amsterdam: North-Holland), 63

Young, T. R., Baron, E., & Branch, D. 1995, ApJ, 449, L51

FIGURE LEGENDS

FIG. 1a.—The $N^*_{\rm Ni}(t)$ deposition curves for a range of t_0 values. The complete trapping curve is a $N^*_{\rm Ni}(t)$ curve with $t_0 = \infty$. The complete escape curve is a $N^*_{\rm Ni}(t)$ curve with $t_0 = 0$. The complete trapping and escape curves are shown on all subsequent deposition curve figures for convenient reference.

FIG. 1b.—The absorption function $f(x)$ (for ^{56}Co) and exponential fits to its inflection point, the point at infinity, and the x-range [2,3]. The fit to the point at infinity is just the constant asymptote which $f(x)$ approaches as $x \to \infty$.

FIG. 2a.—The normalized deposition curve for model W7 calculated with only ^{56}Ni and ^{56}Co and no X-rays (i.e., the limited W7 deposition curve) and the fitted analytic $N^*_{\rm Ni}(t)$ W7 deposition curve.

FIG. 2b.—The same as Fig. 2a, except extending to day 500.

FIG. 3.—The $N^*_{\rm Ni}(t)$ fiducial core-collapse supernova (SN) deposition curve.

FIG. 4a.—The normalized deposition curve for model W7 calculated with all important radioactive species and X-rays included (i.e., the full W7 deposition curve), the limited W7 deposition curve, and the V light curve of SN Ia 1992A. The V light curve has been vertically shifted to fit the deposition curves in roughly the day 300–400 period (which is shown in Fig. 4b). The fit is simply determined by eye.

FIG. 4b.—The same as Fig. 4a, but extending to day 1000.

FIG. 5a.—The UVOIR bolometric light curve of SN II 1987A compared to the $N^*_{\rm Ni}(t)$ fiducial core-collapse supernova (SN) deposition curve. The SN 1987A curve has been vertically shifted to fit the deposition curve in the day 130–200 period. The fit is simply determined by eye.

FIG. 5b.—The same as Fig. 5a, but extending to day 1000.

FIG. 6a.—The schematic SN Ic 1998bw UVOIR bolometric light curve (half-life 44 days) and a fitted $N^*_{\rm Ni}(t)$ deposition curve with fiducial time $t_0 = 134.42$ days.

FIG. 6b.—The same as Fig. 6a, except extending to day 1000.

TABLES

TABLE 1

PARAMETERS FOR THE RADIOACTIVE DECAYS

OF ^{56}Co AND ^{56}Ni

Parameter	^{56}Co	^{56}Ni
$t_{1/2}$ (days)	77.27(3)	6.077(12)
$t_e = t_{1/2}/\ln(2)$ (days)	111.48(4)	8.767(17)
$Q_{\rm total}$ (MeV)	4.566(2)	2.135(11)
$Q_{\rm ph+PE}$ (MeV)	3.74(4)	1.729(17)
$Q_{\rm ph}$ (MeV)	3.62(4)	1.723(17)
$f_{\rm ph}$	0.968(14)	0.996(14)
$f_{\rm PE}$	3.20(16)−2	3.99(18)−3
C (ergs s^{-1} g^{-1})	6.70(7)+9	3.94(4)+10
B (ergs s^{-1} g^{-1})	7.27(7)+9	—

NOTE.—The values have been taken or derived from LBL, Huo 1992, and Browne & Firestone 1986. We have put the uncertainties in the last digits of the parameters in brackets and have written $\times 10^{\pm k}$ as $\pm k$.

The parameters are defined as follows: $t_{1/2}$ is half-life, t_e is e-folding time, $Q_{\rm total}$ is the total energy (including neutrino energy) per decay, $Q_{\rm ph+PE}$ is the mean photon plus PE (positron and decay-ejected atomic electron) kinetic energy per decay, $Q_{\rm ph}$ is the mean photon energy per decay, $f_{\rm ph}$ is the fraction of $Q_{\rm ph+PE}$ in photon energy, $f_{\rm PE}$ is the fraction of $Q_{\rm ph+PE}$ in PE kinetic energy, and C and B are energy generation coefficients specified in the text (see § 3.1). The γ-ray energy from positron annihilation is included in $Q_{\rm ph+PE}$ and $Q_{\rm ph}$. We assume that the neutrinos simply escape the supernova ejecta and make no contribution to the RDE deposition.

TABLE 2
EXPONENTIAL FITS
TO THE ABSORPTION FUNCTION $f(x)$

Fit at x/over $[x_{\rm a}, x_{\rm b}]$ Max. Error (dex) in $[x_{\rm a}, x_{\rm b}]$	$K_{\rm coef}$	$x_{1/2}$	$t_{1/2}^{\rm fid,Ia}$ (days)	$t_{1/2}^{\rm fid,CC}$ (days)
$x = 0$ 0.001 in $[0, 0.40]$ 0.04 in $[0, 0.64]$	1	∞	77.27	77.27
$[0.23, 0.53]$ 0.0033 in $[0.23, 0.53]$	1.027959	7.659517	61.98	75.91
$x = x_{\rm infl} \approx 1.040765$ 0.004 in $[0.8, 1.35]$ 0.04 in $[0.56, 1.82]$	1.950777	0.625347	19.21	63.38
$[0.54, 1.98]$ about $x_{\rm infl}$ (n) 0.014 in $[0.54, 1.98]$	1.694608	0.705462	21.01	64.70
$[0.42, 2.46]$ about $x_{\rm infl}$ (m) 0.028 in $[0.42, 2.46]$	1.540518	0.770151	22.38	65.60
$[0.33, 2.82]$ about $x_{\rm infl}$ (b) 0.04 in $[0.33, 2.82]$	1.441097	0.822176	23.43	66.23
$[2, 3]$ 0.01 in $[2, 3]$	0.804766	1.149675	29.23	69.04
$[4, 8]$ 0.037 in $[4, 8]$	0.151079	4.653005	54.95	75.06
$x = \infty$ 0.098007 in $[2x_{\rm tr}, \infty]$	0.0320	∞	77.27	77.27

NOTE.—The exponential function $K_{\rm coef} \exp(-x/x_e)$ (where x_e is the e-folding reduced time) has been fitted to the absorption function $f(x)$. The fits are either to $f(x)$'s value and its logarithmic slope at a given point x or are fits to $f(x)$ over a given x-range $[x_{\rm a}, x_{\rm b}]$. The point fits are to the asymptotic behavior of $f(x)$ at zero and infinity, and to $f(x)$ at its inflection point $x_{\rm infl}$. A fit to an x-range was chosen so as to reproduce $f(x)$ close to optimally over that range.

The first column gives the point or x-range of the fit in the first line and in subsequent lines the maximum error of the fit (or the maximum deviation of $f(x)$ from the fitted exponential) in specified ranges. The second column gives the coefficient $K_{\rm coef}$ of the fitted exponential, The third column gives the reduced time half-life of the exponential: $x_{1/2} = x_e \ln(2)$. The fourth and fifth columns give the half-lives (in real time) of the product of the ^{56}Co decay exponential and the fitted exponential for the fiducial SN Ia model

and fiducial core-collapse (CC) supernova model posited in §§ 3.3 and 3.4, respectively.

TABLE 3

SUMMARY OF RADIOACTIVE DECAYS IMPORTANT IN MODEL W7

Radioactive species and initial mass					
	Decay	$t_{1/2}$	$Q_{\rm total}$ (MeV)	$Q_{\rm ph+PE}$ (MeV)	$Q_{\rm ph}$ (MeV)
^{44}Ti $1.8\times10^{-5}\,M_\odot$; ^{44}Sc $1.8\times10^{-9}\,M_\odot$					
	^{44}Ti $\rightarrow^{44}$Sc	63(3) years	0.2675(19)	0.1493(15)	0.1384(14)
	^{44}Sc $\rightarrow^{44}$Ca	0.1636(3) days	3.6533(19)	2.73(23)	2.13(23)
^{55}Co $4.5\times10^{-3}\,M_\odot$; ^{55}Fe $1.4\times10^{-3}\,M_\odot$					
	^{55}Co $\rightarrow^{55}$Fe	0.7304(13) days	3.4513(4)	2.43(4)	2.00(4)
	^{55}Fe $\rightarrow^{55}$Mn	2.73(3) years	0.23138(10)	0.0054(3)	0.00163(5)
^{56}Ni $0.58\,M_\odot$; ^{56}Co $6.1\times10^{-5}\,M_\odot$					
	^{56}Ni $\rightarrow^{56}$Co	6.077(12) days	2.135(11)	1.729(17)	1.723(17)
	^{56}Co $\rightarrow^{56}$Fe	77.27(3) days	4.566(2)	3.74(4)	3.62(4)
^{57}Ni $2.15\times10^{-2}\,M_\odot$; ^{57}Co $8.1\times10^{-4}\,M_\odot$					
	^{57}Ni $\rightarrow^{57}$Co	1.4833(25) days	3.264(3)	2.07(3)	1.92(3)
	^{57}Co $\rightarrow^{57}$Fe	271.79(9) days	0.8360(4)	0.1429(8)	0.1253(6)

NOTE.—The masses of the radioactive species are from epoch just after the model W7 explosion (i.e., effectively time zero) (Thielemann et al. 1986; Nomoto et al. 1994b). The nuclear data have been taken or derived from LBL, Huo 1992, Bhat 1992, and Browne & Firestone 1986. We have put the uncertainties in the last digits of the parameters in brackets.

See the note to Table 1 for the definitions of the parameters.

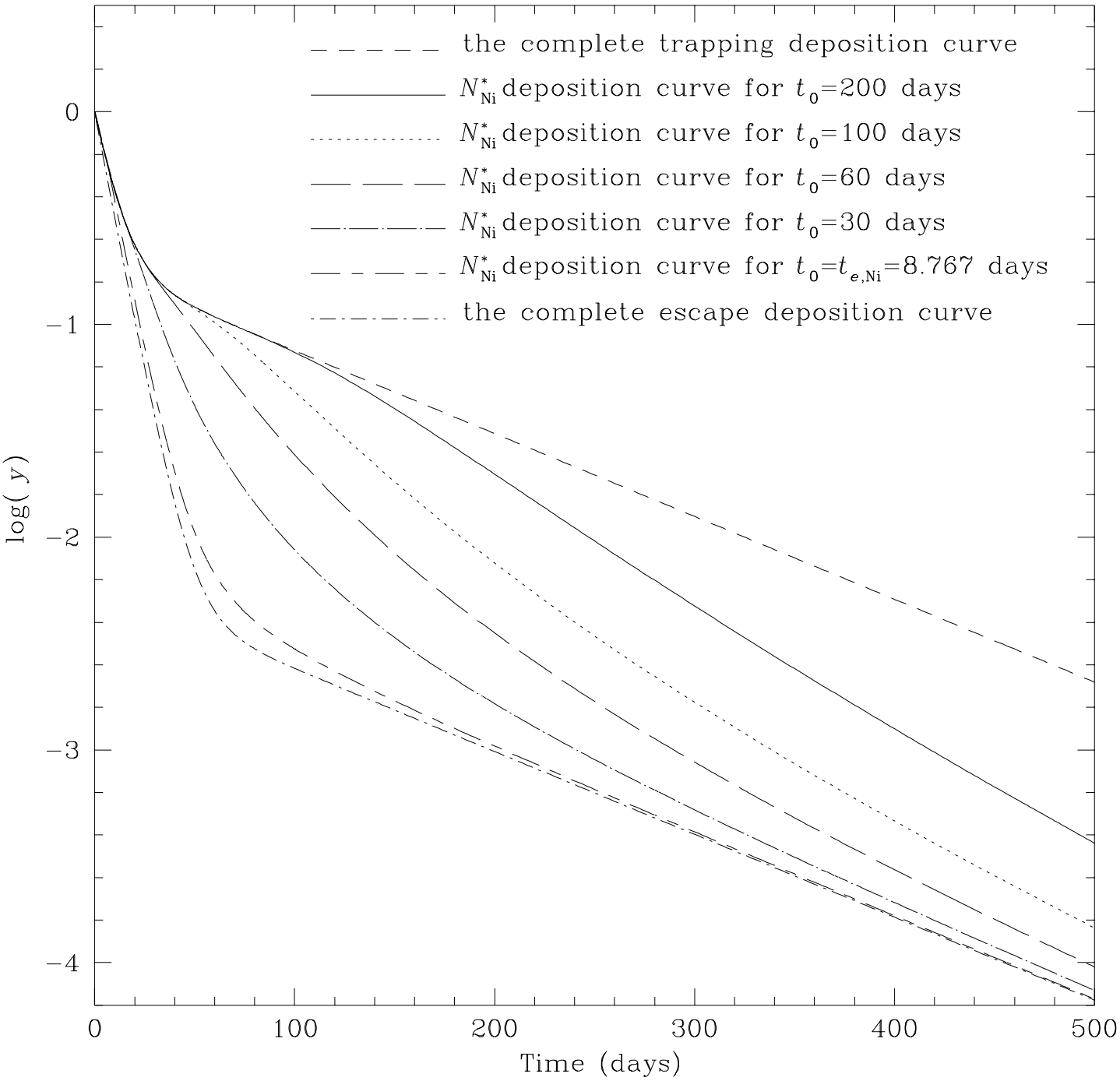
the complete trapping deposition curve
N^*_{Ni} deposition curve for t_0=200 days
N^*_{Ni} deposition curve for t_0=100 days
N^*_{Ni} deposition curve for t_0=60 days
N^*_{Ni} deposition curve for t_0=30 days
N^*_{Ni} deposition curve for $t_0=t_{e,Ni}$=8.767 days
the complete escape deposition curve
log(y)
0
−1
−2
−3
−4
0
100
200
300
400
500
Time (days)

FIG. 1a

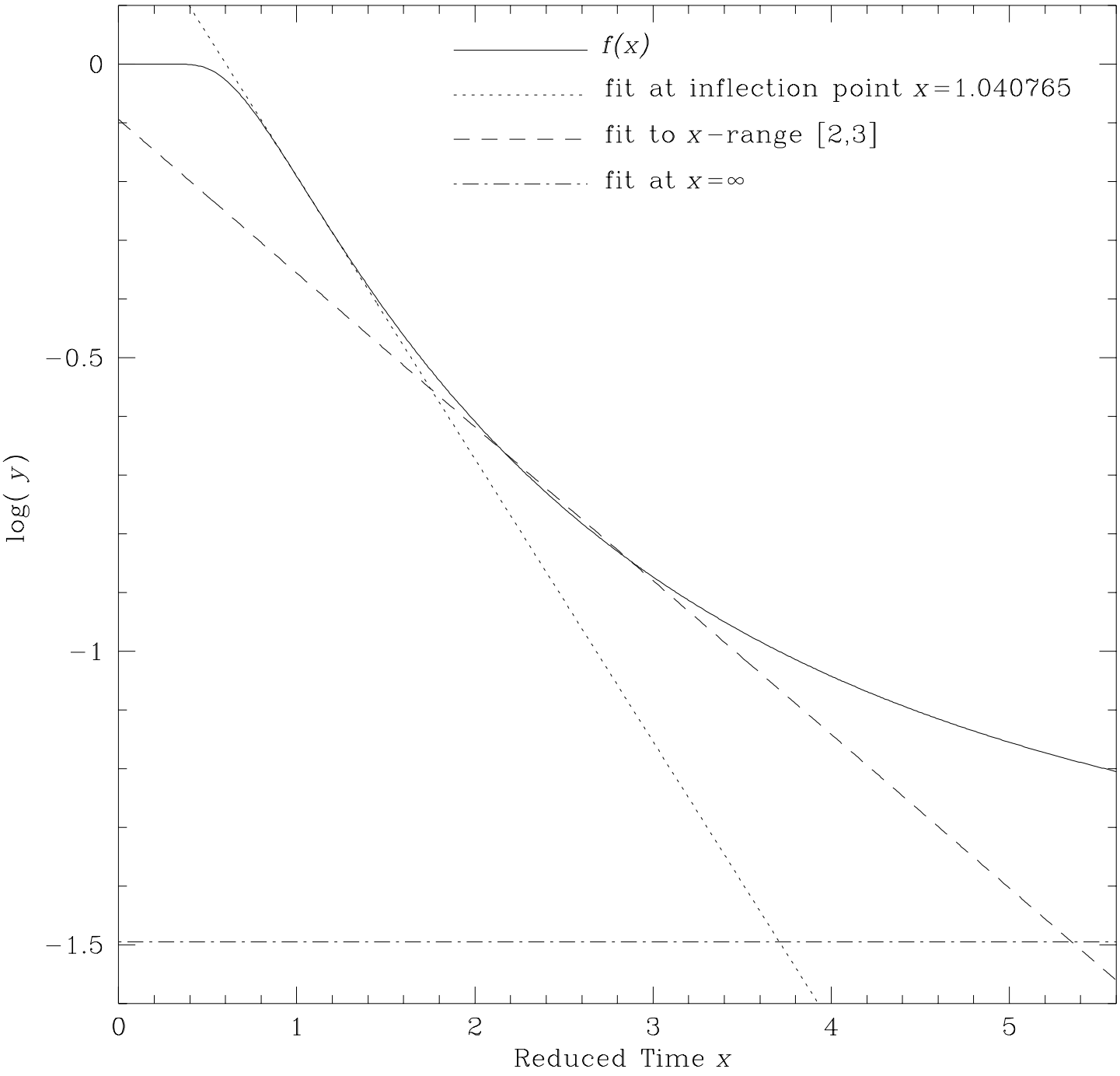
f(x)
fit at inflection point x=1.040765
fit to x−range [2,3]
fit at x=∞
0
−0.5
−1
−1.5
log(y)
0
1
2
3
4
5
Reduced Time x

FIG. 1b

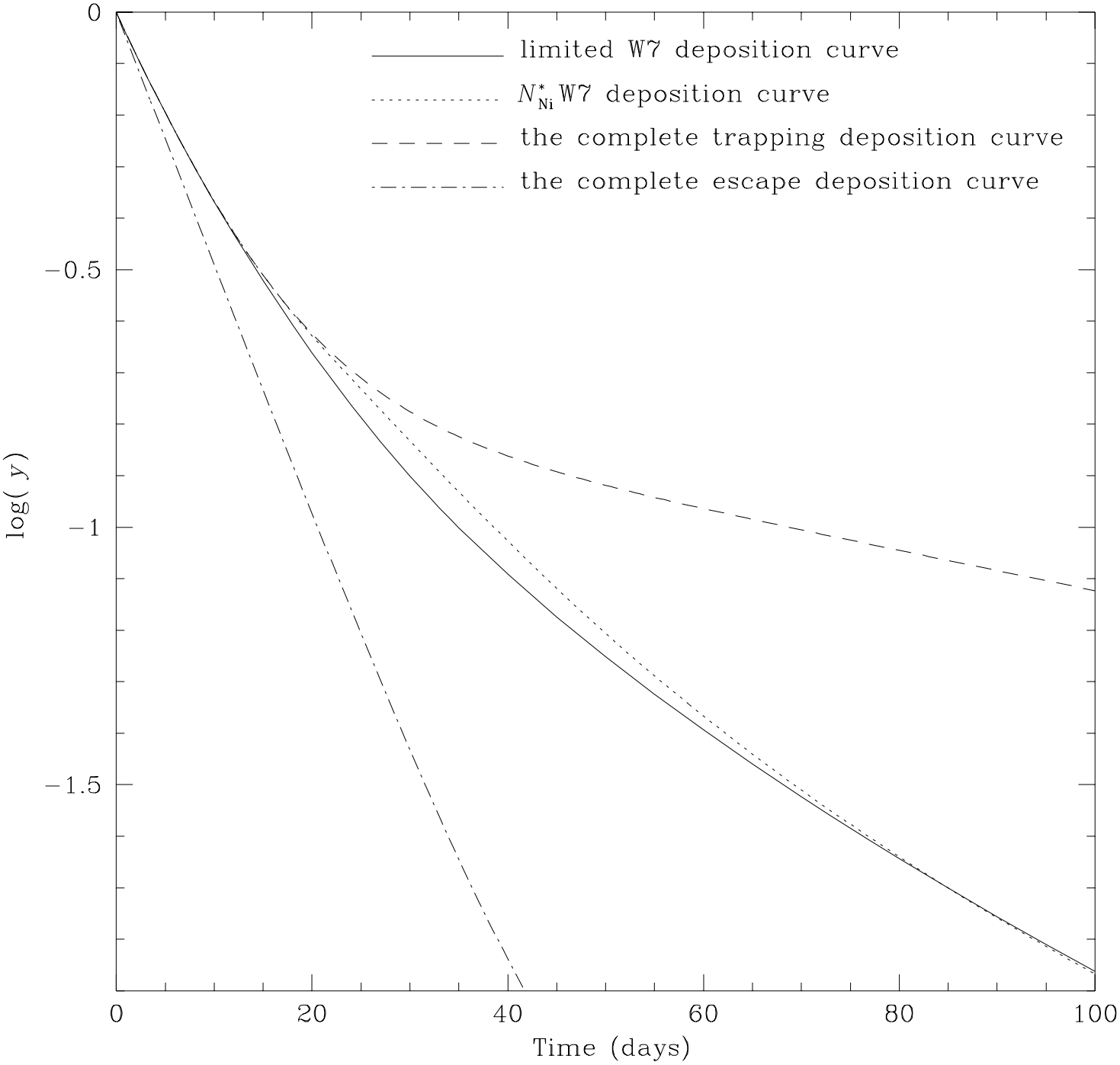
limited W7 deposition curve
N^*_{Ni} W7 deposition curve
the complete trapping deposition curve
the complete escape deposition curve
0
−0.5
−1
−1.5
log(y)
0
20
40
60
80
100
Time (days)

FIG. 2a

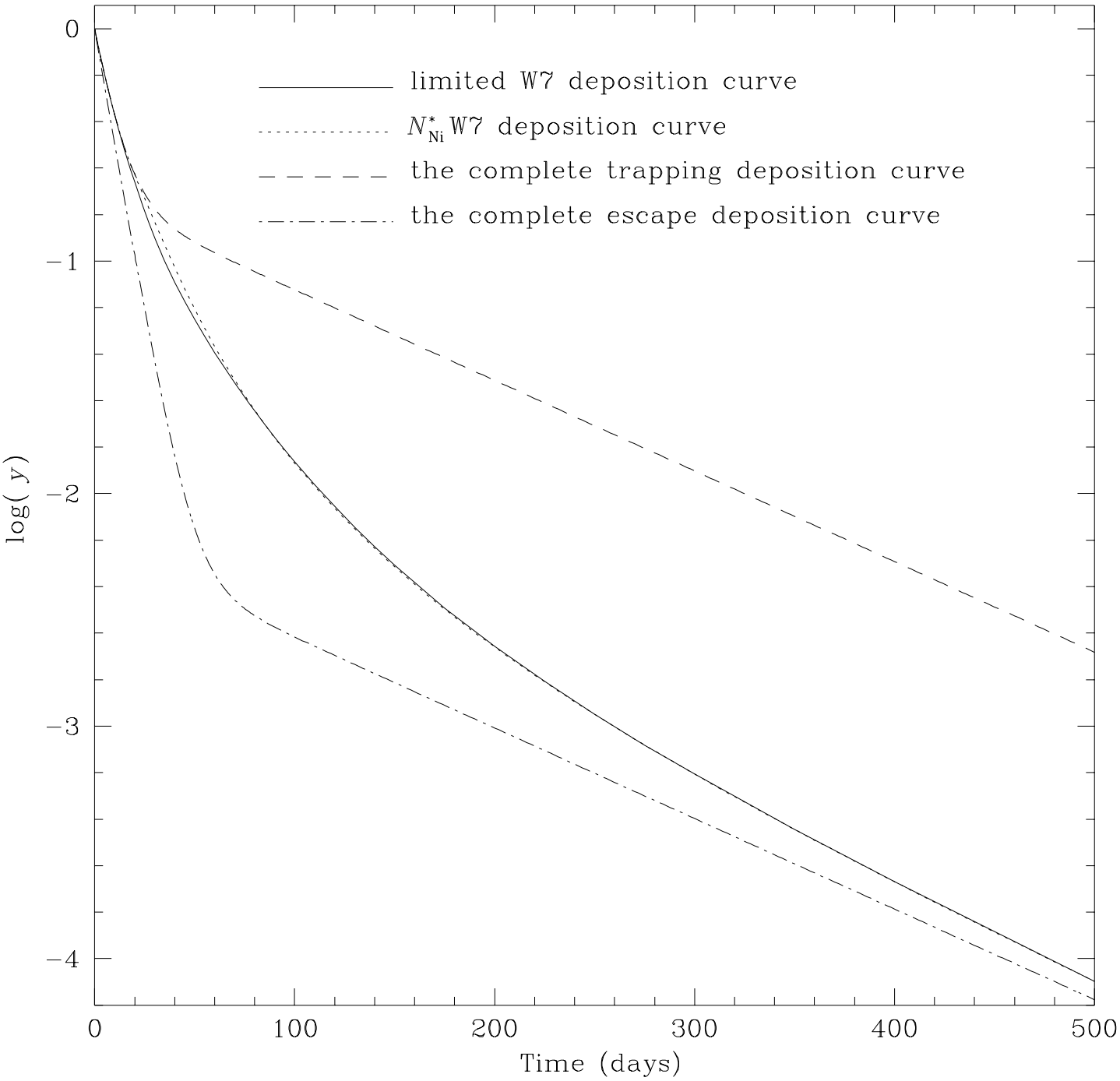
limited W7 deposition curve
N^*_{Ni} W7 deposition curve
the complete trapping deposition curve
the complete escape deposition curve
log(y)
Time (days)
0
−1
−2
−3
−4
0
100
200
300
400
500

FIG. 2b

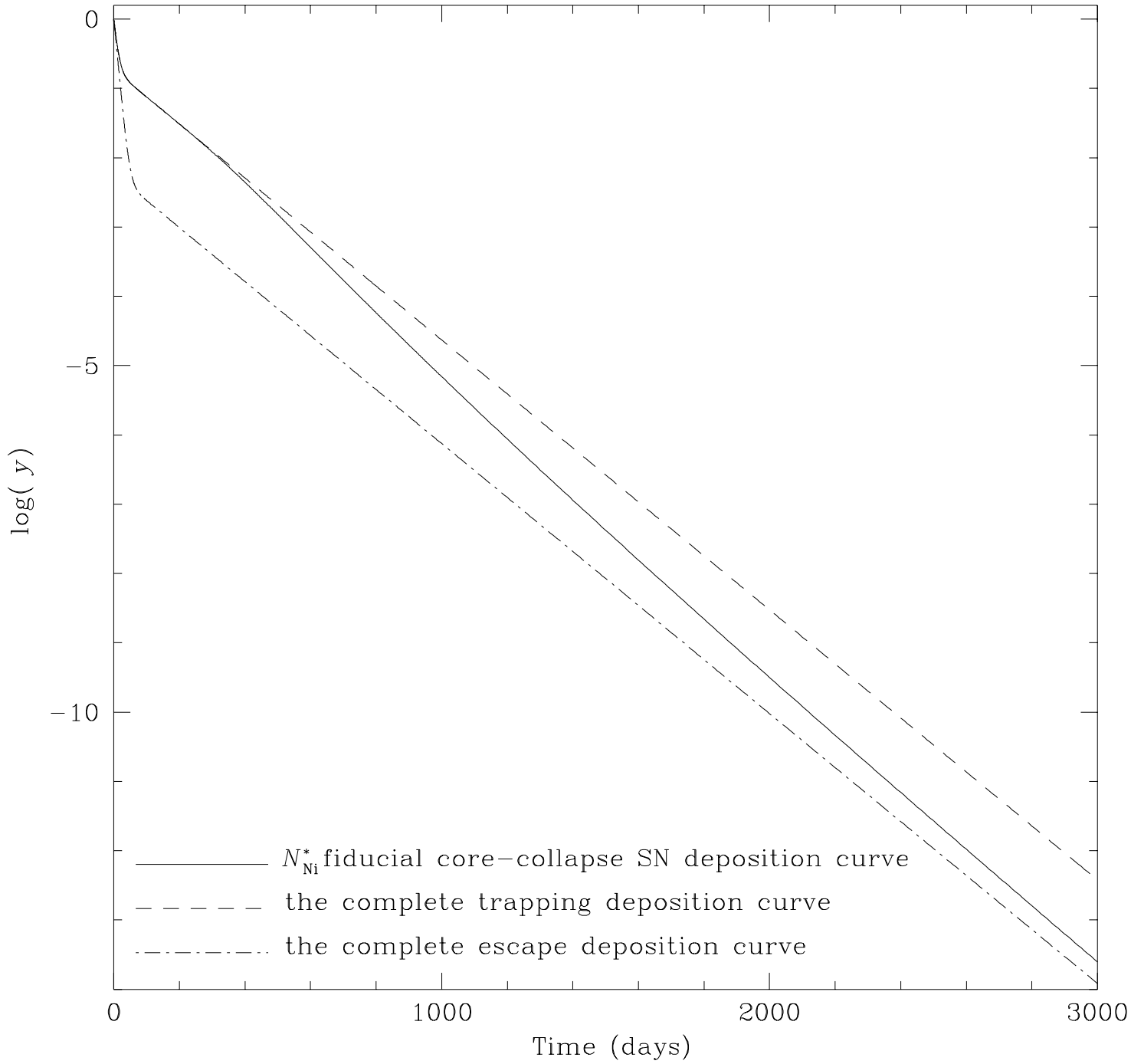
0
−5
−10
log(y)
0
1000
2000
3000
Time (days)
N^*_{Ni} fiducial core−collapse SN deposition curve
the complete trapping deposition curve
the complete escape deposition curve

FIG. 3

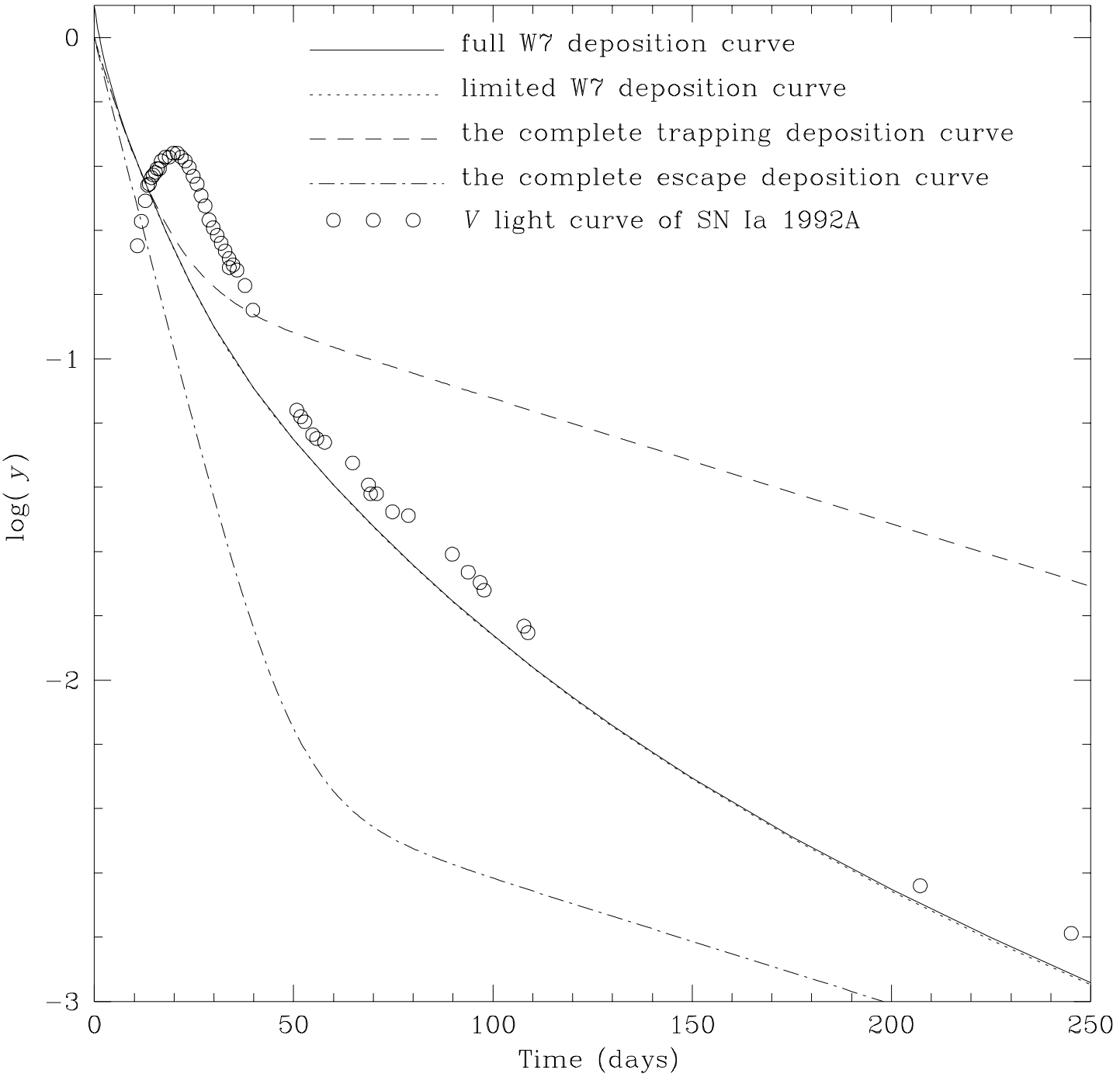
full W7 deposition curve
limited W7 deposition curve
the complete trapping deposition curve
the complete escape deposition curve
V light curve of SN Ia 1992A
0
−1
−2
−3
log(y)
0
50
100
150
200
250
Time (days)

FIG. 4a

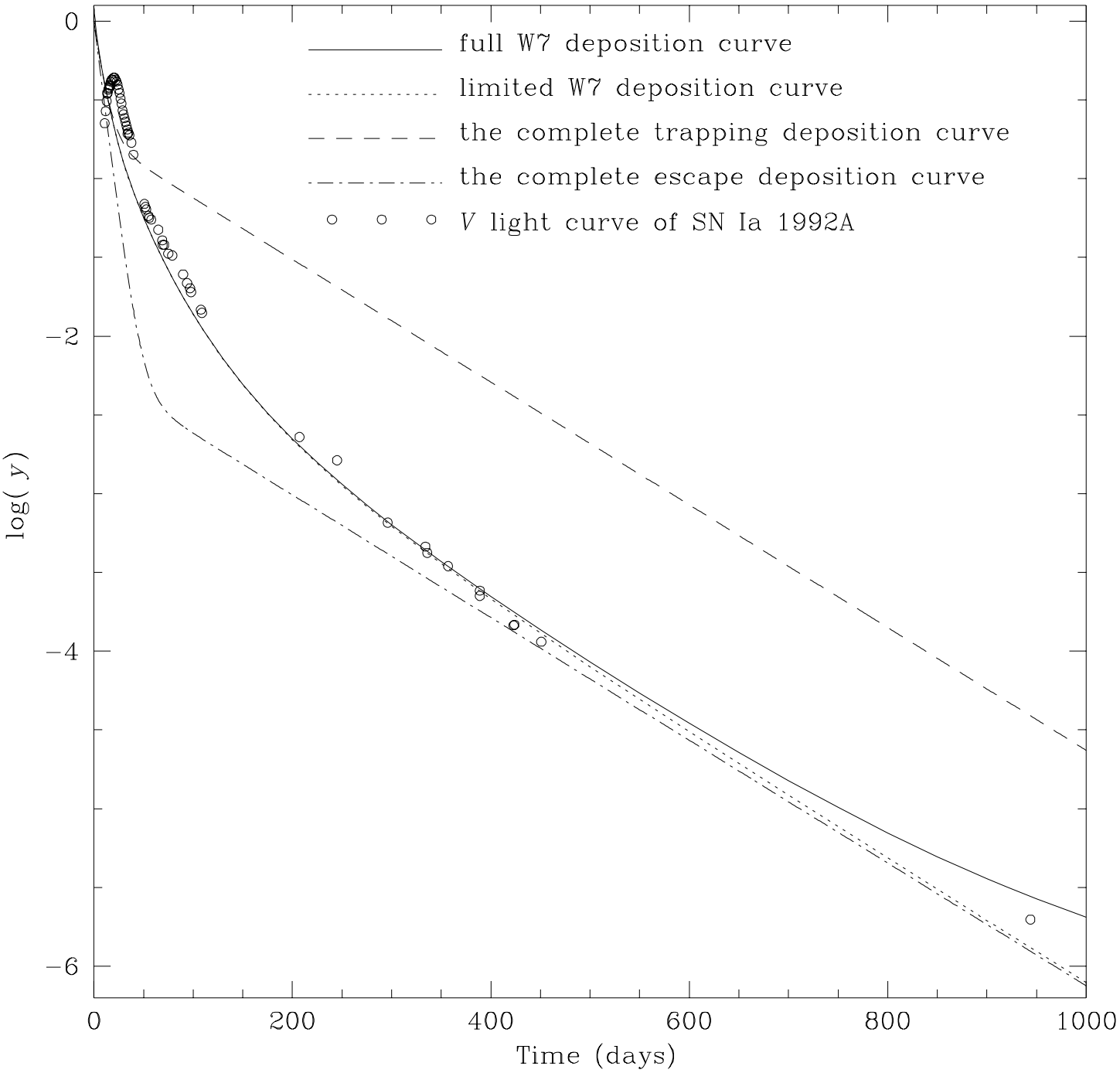
full W7 deposition curve
limited W7 deposition curve
the complete trapping deposition curve
the complete escape deposition curve
V light curve of SN Ia 1992A
log(y)
Time (days)
0
−2
−4
−6
0
200
400
600
800
1000

FIG. 4b

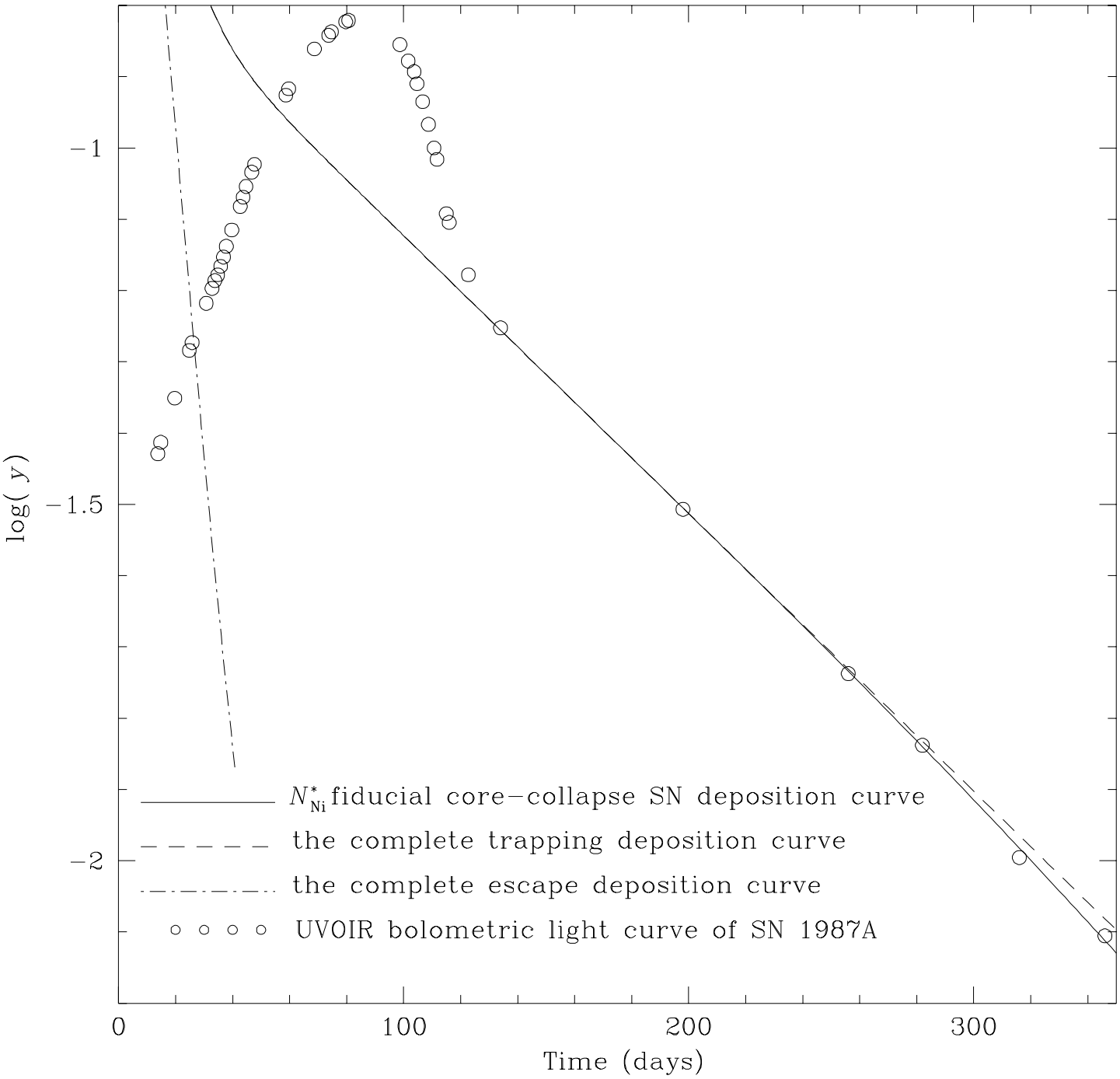
−1
−1.5
−2
log(y)
0
100
200
300
Time (days)
N^*_{Ni} fiducial core−collapse SN deposition curve
the complete trapping deposition curve
the complete escape deposition curve
UVOIR bolometric light curve of SN 1987A

FIG. 5a

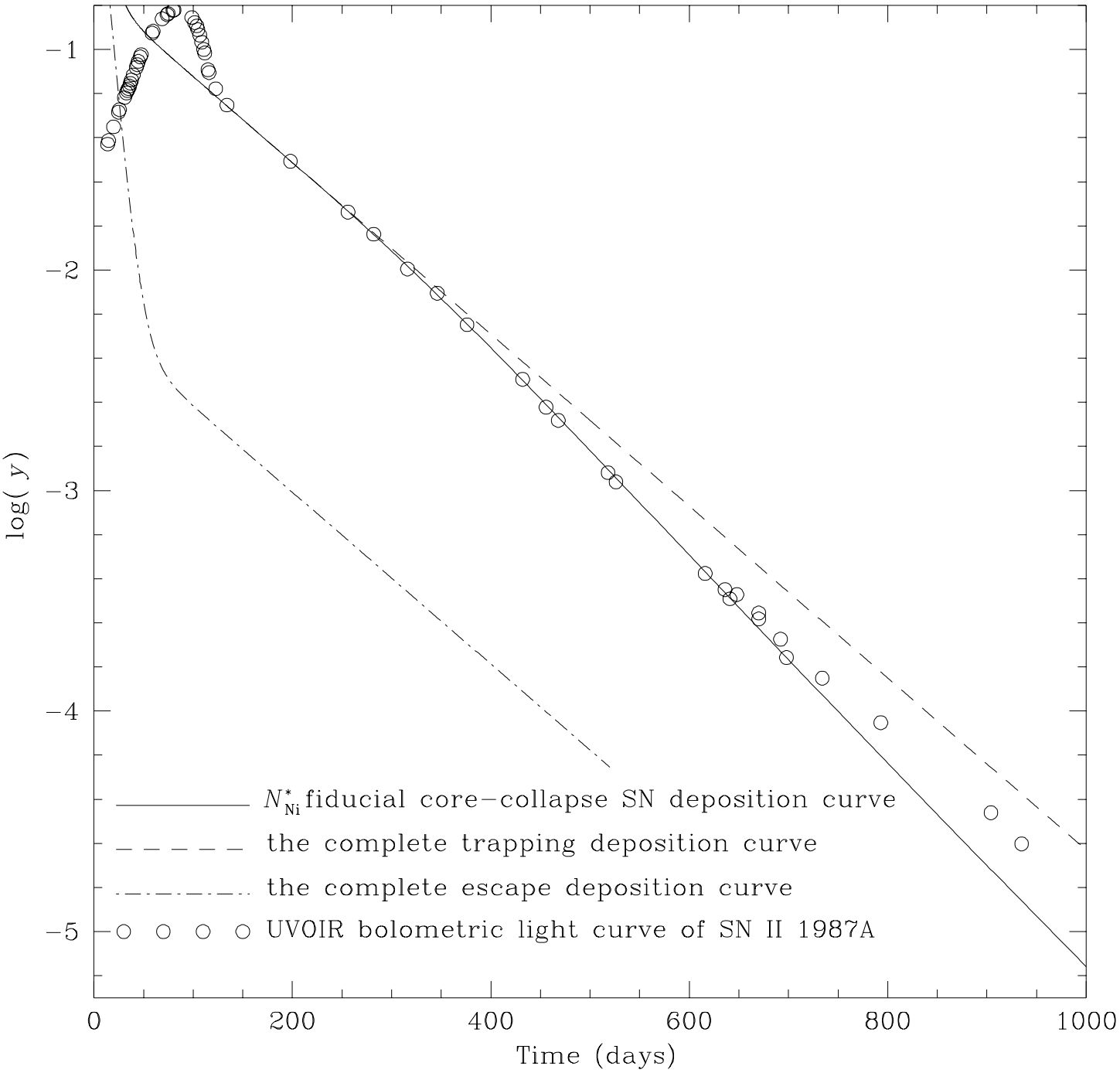
log(y)
−1
−2
−3
−4
−5
0
200
400
600
800
1000
Time (days)
N^*_{Ni} fiducial core−collapse SN deposition curve
the complete trapping deposition curve
the complete escape deposition curve
UVOIR bolometric light curve of SN II 1987A

FIG. 5b

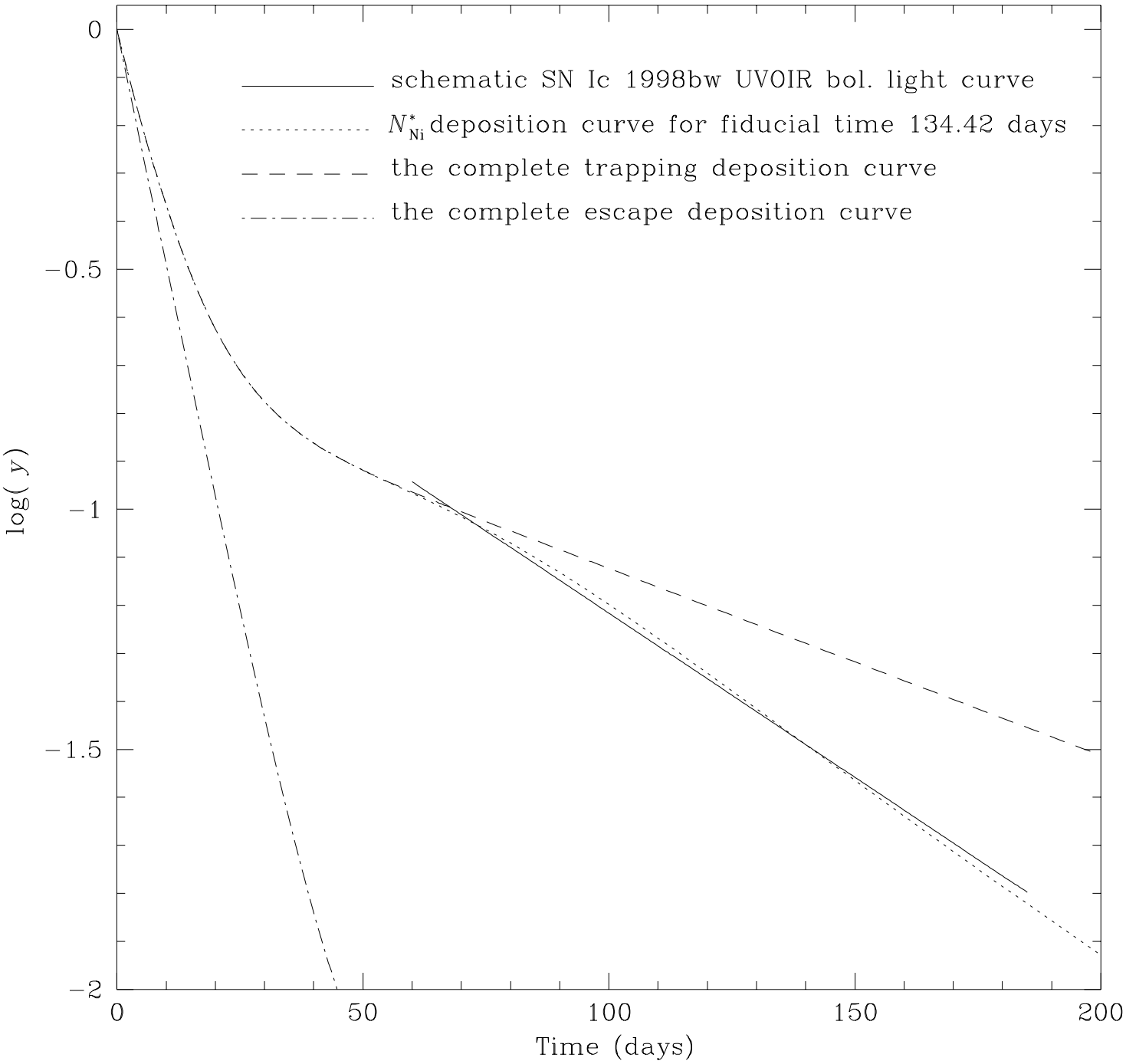
schematic SN Ic 1998bw UVOIR bol. light curve
N^*_{Ni} deposition curve for fiducial time 134.42 days
the complete trapping deposition curve
the complete escape deposition curve
log(y)
Time (days)
0
−0.5
−1
−1.5
−2
0
50
100
150
200

FIG. 6a

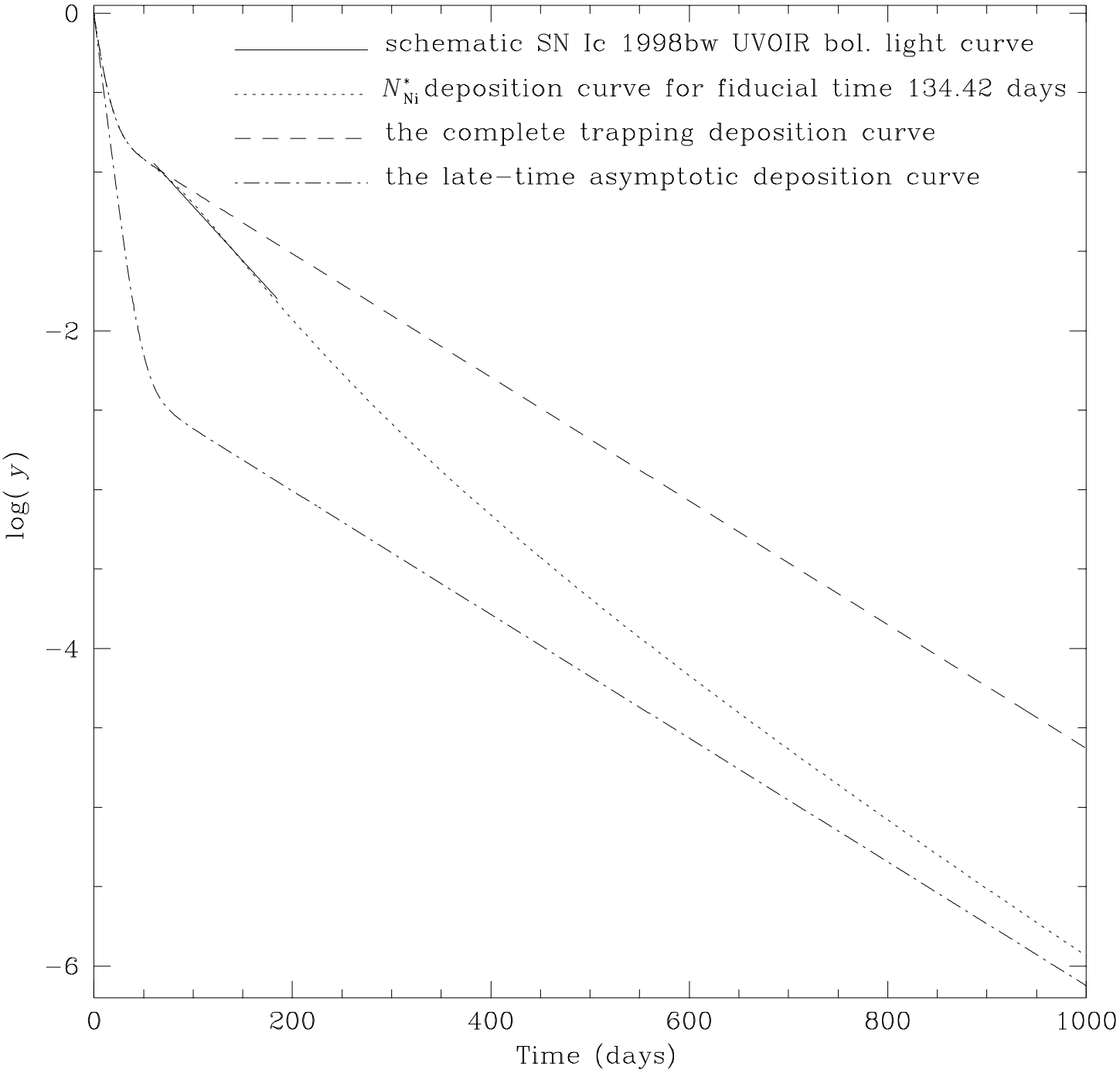
schematic SN Ic 1998bw UVOIR bol. light curve
N^*_{Ni} deposition curve for fiducial time 134.42 days
the complete trapping deposition curve
the late−time asymptotic deposition curve
0
−2
−4
−6
log(y)
0
200
400
600
800
1000
Time (days)

FIG. 6b